Developmental, regenerative, and behavioral dynamics in acoel reproduction

Vikram Chandra[#*], Samantha E. Tseng[#†], Allison P. Kann, D. Marcela Bolaños, Mansi Srivastava*

Department of Organismic and Evolutionary Biology, Museum of Comparative Zoology, Harvard University, 52 Oxford Street, Cambridge, MA 02138

[†] Current address: The Rockefeller University, 1230 York Avenue, New York, NY 10065

# These authors contributed equally.

* Corresponding authors. Emails: vchandra1@fas.harvard.edu, mansi@oeb.harvard.edu

Abstract

Acoel worms belong to an enigmatic and understudied animal lineage in the phylum Xenacoelomorpha. Sparse taxonomic and histological work suggests that these worms exhibit a diversity of reproductive anatomies and likely a corresponding diversity in reproductive behavior. Here, we study the reproductive life history of the three-banded panther worm *Hofstenia miamia*, an acoel that is emerging as a lab-tractable model system. Using confocal microscopy and histology, we describe *H. miamia*'s reproductive organs, identifying structures previously unknown in acoels. Following a cohort of worms from zygote to adulthood, we quantify the developmental dynamics of their reproductive organs, and find that these organs emerge in a stereotyped sequence as a function of increasing body size. Studying the dynamics of organ growth and de-growth during regeneration and in starvation, we show that reproductive organs follow similar growth rules in these contexts, suggesting that they are regulated by a size-

associated program in all growth contexts. Finally, we study egg-laying behavior, finding that *H. miamia* lay their eggs through their mouths after loading them into their pharynges. Worms lay eggs for multiple months after a single mating, suggesting long-term sperm storage despite lacking a storage organ; we also find that worms can lay viable eggs without mating, indicating a capacity for self-fertilization. Further, we show that worms assess their environment to make decisions about when and where to lay their eggs, and sometimes lay eggs in communal clutches. Together, our work establishes foundational knowledge to enable the experimental study of reproductive anatomy, physiology, and behavior in acoels.

Introduction

Reproduction is critical for evolutionary success, and animals display great diversity in their reproductive life histories. The anatomical structures and life history strategies employed for reproduction have been relatively well-studied in some animal lineages, such as arthropods and vertebrates (Davies et al., 2013). However, a full understanding of reproductive biology is lacking in many animal phyla. For example, Phylum Xenacoelomorpha, which includes acoels, nemertodermatids, and xenoturbellids, is an early branching bilaterian lineage of primarily marine worms whose life histories are largely unknown (Bock, 1923; Bourlat and Hejnol, 2009; Cannon et al., 2016; Kapli and Telford, 2020; Philippe et al., 2011) (Fig. 1A).

Roughly 400 species of acoel worms have been described (Achatz et al., 2013; Jondelius et al., 2011; Tyler, S., Schilling, S., Hooge, M., & Bush, L. F., 2012; Wallberg, 2012). Analyses of histological sections of specimens collected in the field suggest that, with few exceptions (Crezée, 1975; Mamkaev, 1965; Raikova et al., 1995), acoels are simultaneous hermaphrodites. Unlike many marine animals that reproduce sexually through spawning and external fertilization, e.g., cnidarians, poriferans, echinoderms, etc. (Giribet and Edgecombe,

2020), acoels have been reported to reproduce sexually through internal fertilization (Achatz et al., 2013). They exhibit a striking diversity in their reproductive anatomy (Table S1). This anatomical variation likely accompanies variation in reproductive physiology and behavior. While a few species have been cultured in the lab (Bailly et al., 2014; De Mulder et al., 2009; Shannon and Achatz, 2007; Zauchner et al., 2015), little is known about how acoels develop their reproductive organs, mate, or lay eggs.

To improve our understanding of acoel life histories, we studied reproduction in a lab tractable species, the three-banded panther worm *Hofstenia miamia* (Fig. 1B,C). *H. miamia* is a new research organism with features that allow us to study it in controlled conditions: its life cycle can be closed in the lab (worms develop from embryo to gravid adult in 2-3 months), and there is a growing array of experimental tools to observe and manipulate the worms (Gehrke et al., 2019; Hulett et al., 2023; Kimura et al., 2022, 2021; Ricci and Srivastava, 2021; Srivastava, 2022). Histology-based work has described the coarse anatomy of reproductive organs in animals in the genus *Hofstenia* (Beltagi and Mandura, 1991; Bock, 1923; Corrêa, 1960; Hooge et al., 2007; Hookabe et al., 2024; Steinböck, 1966). However, the fine structure of these organs, how they grow and develop, and how they function in the course of reproductive behavior remains unknown. To address these questions about the reproductive life history of *H. miamia*, we use a combination of confocal microscopy, fluorescence *in situ* hybridization, immunofluorescence, and histology, as well as observations of reproductive development and behavior in controlled conditions. We reveal new facets of acoel reproductive biology, show that active processes of growth and destruction ensure coordinated organ development and regeneration, and establish a foundation for the mechanistic study of reproduction in acoels.

Results

An overview of *Hofstenia miamia*'s reproductive anatomy

The genus *Hofstenia* (Bock, 1923) lies within the family Hofsteniidae. The family currently contains four genera (Ahyong et al., 2024; Hookabe et al., 2024) and is an early-branching lineage within acoels (Abalde and Jondelius, 2024; Jondelius et al., 2011). Three species are currently recognized within the genus *Hofstenia*: *H. atroviridis*, *H. miamia*, and *H. arabiensis* (Ahyong et al., 2024; Beltagi and Mandura, 1991; Bock, 1923; Corrêa, 1960; Hooge et al., 2007). Like other acoels, *Hofstenia* are considered to be simultaneous hermaphrodites (Beltagi and Mandura, 1991; Bock, 1923; Corrêa, 1960; Hooge et al., 2007; Steinböck, 1966). *Hofstenia miamia* is likely the most common and widespread species within the genus, with a geographic distribution in the Caribbean and the North Atlantic, including the Bahamas and the Florida coast (Beltagi and Mandura, 1991; Bock, 1923; Corrêa, 1960; Hooge et al., 2007; Steinböck, 1966). All three *Hofstenia* species are described as having an anterior male reproductive system including a seminal vesicle, prostatic vesicle (historically called the *vesicula granulorum* (Bock, 1923) or granule vesicle (Hooge et al., 2007)), a penis with sclerotized needles, 'diffuse' testes, and a ventral male gonopore near the mouth (Beltagi and Mandura, 1991; Bock, 1923; Corrêa, 1960; Hooge et al., 2007; Steinböck, 1966). The female reproductive system, as described, includes two ovaries spanning the posterior two-thirds of the worm. However, these descriptions were all based on worms roughly 5-8mm in length (Beltagi and Mandura, 1991; Bock, 1923; Corrêa, 1960; Hooge et al., 2007; Steinböck, 1966). In our lab cultures, fully grown adult *H. miamia* can be over 1.4cm in length. We noticed that these large adults were more likely to reproduce than smaller worms, and we reasoned that their anatomy could also be different. We therefore began by re-examining the coarse anatomy of *Hofstenia miamia*.

101 We anesthetized adult worms, mounted them ventral side up on a slide, and imaged them
102 through a dissecting microscope and found, as expected, that *H. miamia*'s male copulatory
103 structures are located in the anterior of the animal, just posterior to the mouth (Fig. 1C,D; Fig.
104 S1A). These male structures are located within a translucent cylindrical region close to the
105 ventral surface of the worm and immediately ventral to the pharynx. We observed two opaque,
106 white regions within the male copulatory apparatus, located towards its posterior (Fig. 1C; Fig.
107 S1A). The larger, posterior oval structure corresponds to the seminal vesicle, while the smaller,
108 teardrop-shaped anterior structure corresponds to the prostatic vesicle (Fig. 1C,D; Fig. S1A)
109 (Beltagi and Mandura, 1991; Bock, 1923; Corrêa, 1960; Hooge et al., 2007; Steinböck, 1966).
110 Previous work reported that *H. miamia* has a penis (Fig. S1A): a sperm-delivery organ
111 containing rigid needles known as 'stylets' (Hooge et al., 2007; Steinböck, 1966). Although
112 stylets are difficult to see in this imaging preparation, we identified a small aperture immediately
113 posterior and ventral to the mouth (Fig. S1A), and we observed that the worm extended its
114 penis through it, showing that this aperture is the male gonopore and confirming the location of
115 the penis in the anterior of the worm. As previously described (Beltagi and Mandura, 1991;
116 Bock, 1923; Corrêa, 1960; Hooge et al., 2007; Steinböck, 1966), we found that the female
117 reproductive system occupies the posterior two-thirds of the worm (Fig. 1C,D; Fig. S1B). This
118 system consists of numerous eggs grouped into three distinct clusters: one lateral group on
119 each side of the body extends along the anterior-posterior axis (Fig. S1B), and a medially-
120 located cluster lies just posterior to the pharynx (Fig. S1C). The lateral clusters contain oocytes
121 of various sizes, likely corresponding to different stages of maturation. These oocyte-laden
122 regions in the parenchyma have been identified as the ovaries in historical reports (Beltagi and
123 Mandura, 1991; Bock, 1923; Corrêa, 1960; Hooge et al., 2007; Steinböck, 1966). Posterior to
124 the pharynx, there is often a cluster of uniformly sized, spherical eggs that do not have a
125 germinal vesicle (Fig. 1C,D; Fig. S1C). The number of eggs at this position is highly variable,
126 ranging from zero to over a dozen eggs. In *H. atroviridis*, Bock (1923) speculated that these

127 eggs are mature, fertilized, and ready to be laid: i.e., zygotes. To test whether these eggs were
128 indeed zygotes, we dissected out eggs from this medial cluster, as well as from the lateral
129 ovaries. We found that 46/56 eggs (removed from the medial clusters of 9 worms) developed
130 and hatched into juvenile worms, in line with previously established developmental timing (Fig.
131 S1D) (Kimura et al., 2021). Meanwhile, all eggs dissected from the lateral ovaries disintegrated
132 within 48 hours. The eggs in this medial cluster are therefore mature, likely fertilized, and ready
133 for laying, while eggs in the ovaries are immature and likely unfertilized. Overall, these
134 observations confirm and extend previous descriptions of *H. miamia*, and provide a high-level
135 overview of its reproductive anatomy. Next, taking advantage of *H. miamia*'s tractability, we
136 sought to obtain a finer understanding of its reproductive structures and their development.
137
138
139 **Dynamics of reproductive organ development**
140 How reproductive structures develop as animals reach sexual maturity is not well understood in
141 the Xenacoelomorpha. As in the acoel *Aphanostoma pulchra* (previously *Isodiametra pulchra*)
142 (Chiodin et al., 2013), hatchling *H. miamia* have no visible reproductive structures, and previous
143 observations suggested that these develop over a month after hatching as the worms grow
144 toward adulthood (Kimura et al., 2021; Srivastava, 2022). To determine the timeline and
145 dynamics of reproductive development, we reared 42 zygotes in isolation and monitored their
146 growth over time (Fig. 1E,F), precisely controlling their rearing environment such that each
147 animal had access to defined amounts of seawater and food (see Methods). To assess whether
148 nutrition affects reproductive development, we split the cohort of hatchling worms into two
149 groups that were fed differently. For each group, we gradually increased the amount of food
150 they were given as they grew larger, to ensure that worms always had *ad libitum* food access
151 while avoiding unnecessary overfeeding. These food increases occurred periodically, but we
152 delayed them by two weeks for one feeding group (Fig. S2A,B). We reasoned that this

153 treatment would delay growth in one group, allowing us to decouple biological age from organ
154 and body growth. Twice weekly, we captured images of the ventral surface of each worm and
155 quantified the size of each visible reproductive structure.
156
157 We found that worms maintained their aspect ratios from hatchling to adult, growing
158 proportionally over time (Fig. 1E-H; Fig. S2C). At every stage of development, the size of each
159 reproductive organ scaled with body size once that organ appeared (Fig. 1I-K). Worms with
160 delayed increases in feeding displayed corresponding delays in their growth, both in their body
161 size (Fig. S2D) and in the timing of appearance of their ovary and seminal vesicle (Fig. 1L). The
162 penis and seminal vesicle developed at a smaller size in these worms compared to worms
163 without delayed feeding increases (Fig. 1M), suggesting that resource-limited worms may invest
164 disproportionately in male development. Multiple regression found that organ size was
165 explained by both age and body size, but that body size was a better predictor of the size of
166 each reproductive organ (Table S2). This suggests that the differentiation and growth of
167 reproductive structures is coupled to the worm's body size, rather than to its age.
168
169 We found that reproductive development generally occurs in a stepwise fashion, where organs
170 appear in a consistent sequence at serially increasing body sizes. Newly hatched animals
171 possess all major somatic organs (such as a brain, muscle system, pharynx, gut, etc. (Kimura et
172 al., 2022, 2021)), but lack all reproductive structures (Fig. 1E,F). 4-6 weeks after egg laying,
173 when the worm is about 3 ± 0.6 mm (mean ± SD) in length, the anterior-ventral tissue housing
174 the future male copulatory apparatus becomes visibly less dense, and a groove becomes
175 apparent in the ventral surface. Soon after, the male gonopore becomes detectable posterior to
176 the mouth. Sperm begin to accumulate in the seminal vesicle around 35 days post laying, once
177 a worm is about 4.4 ± 0.9 mm (mean ± SD) long. Shortly after, when a worm is 5.6 ± 0.9 mm
178 (mean ± SD), the first oocytes become visible in nascent ovaries. These ovaries grow with the

179 worm over time, with existing oocytes maturing and new ones continuously added. Around two
180 months after being laid, typically after a worm is 8.7 ± 1.2 mm in length, eggs appear near the
181 base of the pharynx (Fig. 1E,F,L,M). These eggs are laid within hours or days, and they develop
182 and hatch into juvenile worms. Given that these worms were isolated since birth, this suggests
183 that *H. miamia* can reproduce through self-fertilization.
184
185 To visualize the extent to which reproductive structures develop in sequence, we ranked each
186 structure in each worm by its date of appearance (Fig. 1N). All worms, without exception, first
187 developed a penis. A few worms simultaneously developed a seminal vesicle; in most other
188 worms, this structure appeared second, with a few developing their seminal vesicle concurrent
189 with nascent ovaries. Ovaries always appeared before the first fertilized eggs were seen in the
190 central region. Next, we asked whether the left and right ovaries of each worm developed in
191 synchrony. We found that on the first day that an ovary was visible, 34/34 worms had both
192 ovaries visible. Partial regression analysis revealed that the sizes of the two ovaries within a
193 worm are strongly correlated, even when correcting for body size (Fig. S2E). Consistent with
194 findings from bilaterally-symmetric organs in other animals (Allard and Tabin, 2009; Boulan and
195 Léopold, 2021; Harris et al., 2021; Vallejo et al., 2015; Wolpert, 2010), this suggests that an
196 active process may synchronize ovarian growth within individual worms.
197

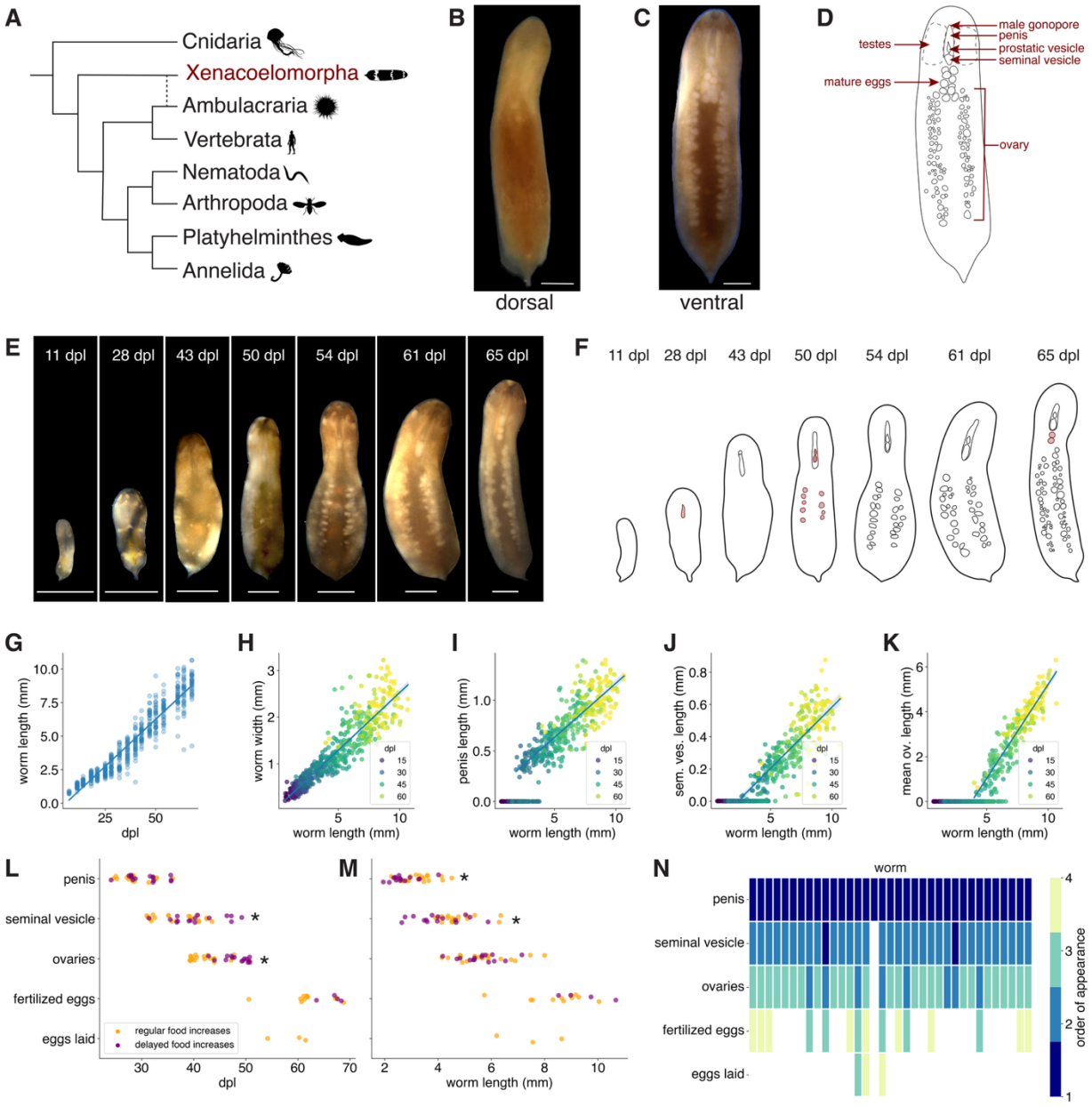

Figure 1: Reproductive organs develop in a size-associated sequence. (**A**) Xenacoelomorpha is an early-branching bilaterian lineage of aquatic worms. Phylogeny modified from (Srivastava, 2022). Animal icons are from phylopic.org, and are in the public domain; the dashed line reflects uncertainty in the consensus phylogeny (Cannon et al., 2016; Kapli and Telford, 2020; Philippe et al., 2011). (**B**) Dorsal view of an adult *Hofstenia miamia*. (**C**) Ventral view of an adult *Hofstenia miamia*; most reproductive structures are visible in this view. (**D**) Schematized view of the ventral surface of a worm with known reproductive structures illustrated. (**E**) Timecourse of a representative worm through development, from

206 hatchling to reproductively mature adult. (**F**) Schematic of timecourse shown in (**E**) with key reproductive
207 developments illustrated. The first appearance of each organ is highlighted in red. (**G**) The length of
208 worms increases over time ($R^2 = 0.91$, $p < 0.0001$), and (**H**) worms grow proportionally: their length scales
209 with their width ($R^2 = 0.85$, $p < 0.0001$). Error band shows 95% confidence interval. (**I-K**) The length of
210 each reproductive organ scales with increases in body size (penis: $R^2 = 0.70$, $p < 0.0001$; seminal vesicle:
211 $R^2 = 0.63$, $p < 0.0001$; ovaries: $R^2 = 0.84$, $p < 0.0001$). Error band shows 95% confidence interval, with
212 zero values excluded from these regressions. (**L**) Worms with delayed feeding increases had significant
213 delays in the appearance of their seminal vesicle and ovaries, but not the penis (Welch's t test for date of
214 appearance for penis: $p = 0.08$, seminal vesicle: $p = 0.04$, ovary: $p < 0.0001$; $n \geq 15$). (**M**) Worms with
215 delayed feeding increases had a smaller body length when a penis and seminal vesicle appeared, but not
216 when ovaries appeared (Welch's t test for length on date of appearance for penis: $p = 0.005$, seminal
217 vesicle: $p = 0.03$, ovary: $p = 0.74$; $n \geq 15$). Asterisks indicate statistical significance. (**N**) Ranking the order
218 in which reproductive organs appear (y-axis) in developing worms reveals a stepwise pattern of
219 reproductive differentiation. The x-axis shows individual worms. dpl = days post laying. Scale bars: 1 mm.
220

221 **De-growth and regeneration of reproductive organs**

222 Next, we asked whether these patterns of growth persisted in different contexts. *H. miamia*, like
223 other studied acoels, is an excellent regenerator and can regenerate all tissues from a wide
224 range of initial tissue configurations (Srivastava, 2022; Srivastava et al., 2014; Steinböck, 1966).
225 We amputated and followed adult worms in three ways: by isolating tail tips (which contain no
226 reproductive structures) and studying how they regenerated the majority of their organs, by
227 cutting worms sagittally and studying how they regenerated their missing half, and by isolating
228 heads from tails and studying how these head fragments regenerated their tails and the
229 posterior region of their ovaries (Fig. 2A). Head and tail tip fragments both gradually increased
230 in size, with tail tip fragments growing much faster in size (Fig. S3A-G). Within two weeks, most
231 of these fragments had regained the characteristic shape of intact worms. Sagittally-cut

232 fragments first shrank in size before subsequently growing (Fig. S3G), and appeared to take
233 longer to fully regain normal worm-like appearance (Fig. S3C,D). All reproductive organs
234 gradually regenerated, with growth dynamics contingent on the nature of the injury (Fig. 2B-J;
235 Fig. S3A-F,H,I). Additionally, we asked how reproductive organs change in another context:
236 degrowth. Anecdotal observations suggested *H. miamia* tolerates long periods of starvation but
237 gradually shrinks in size when deprived of food. We used this starvation-induced de-growth to
238 ask whether reproductive organs scale with decreasing body size. We starved a cohort of adult
239 worms and quantified the de-growth of their reproductive organs over time (Fig. 2K,L). We found
240 that all worms survived over three months of continuous starvation, gradually shrinking over
241 time (Fig. 2M). Worms maintained their aspect ratios as they shrank (Fig. 2K,L,N), and their
242 reproductive organs shrank correspondingly (Fig. S4A-E). Partial regression analysis of
243 shrinking ovaries showed that they shrink synchronously (Fig. S4F), suggesting active
244 coordination of de-growth across the left-right axis.
245
246 The stepwise growth relationships we found between reproductive organs and body size during
247 post-embryonic development largely generalized to both regeneration and de-growth (Fig. S4G-
248 I). Starving worms lost most reproductive organs in the opposite order to which they developed
249 them, first losing fertilized eggs, then ovaries, and eventually losing their seminal vesicle (Fig.
250 2O,P). However, after three months of starvation, most worms continued to retain their penes
251 despite being below the threshold size at which we would expect to see loss of this organ (Fig.
252 2O), perhaps because rigid, sclerotized structures degrade differently from soft tissue. In
253 regenerating tail tip fragments, the male reproductive structures generally developed before the
254 female reproductive structures, following similar stepwise patterns to developing juvenile worms
255 (Fig. 2Q). Scaling coefficients for each organ were statistically distinguishable across
256 development, regeneration, and de-growth, but the effect sizes of the differences between
257 coefficients were generally small (Fig. S4G-I, Table S3). Analyzing this effect in more detail, we

found that unsurprisingly, amputated worms initially display aberrant organ scaling but recover typical scaling as they regenerate (Fig. S4J-L). Qualitatively, across all of these growth contexts, reproductive organs scaled with body size in similar ways (Fig. S4G-I, Table S3).

In sagittally-cut worms, each worm fragment retained one of its two ovaries immediately after amputation. These ovaries first partially degenerated before growing back (Fig. 2G; Fig. S3C,D), consistent with the reported loss of germline tissue during early regeneration in heads regrowing tails (Hulett et al., 2023). Body size also decreased after sagittal amputation (Fig. S3G), but ovarian degrowth was disproportionate (Fig. S4M). The rate of ovarian degrowth (normalized to body size) was also significantly greater than the rate of normalized ovarian degrowth during starvation (Fig. S4M). Consistent with studies showing extensive cell death during early regeneration in other systems (Ballarin et al., 2008; Pellettieri et al., 2010; Rychel and Swalla, 2008), this suggests that an active destructive process is responsible for degrowth during ovary regeneration in acoels. The missing ovary began to grow back roughly one month after amputation. We found that the ovaries grew asymmetrically in these worms, with the new ovary growing faster (Fig. 2G). This suggests the existence of an active growth mechanism to ensure that both ovaries reach a symmetric target size.

Together, our results suggest the existence of a size-associated program that regulates the development of reproductive organs, as well as active tissue growth and destruction mechanisms to achieve organ symmetry. It is likely that this program regulates reproductive organ growth in a variety of different developmental contexts, including the transition from juvenile to adult worm, regeneration after injury and tissue loss, and during starvation-induced de-growth. With this high-level understanding of male and female reproductive system anatomy and the scaling relationships that govern their formation in hand, we next sought to understand these systems at higher resolution in order to decipher their functional morphology.

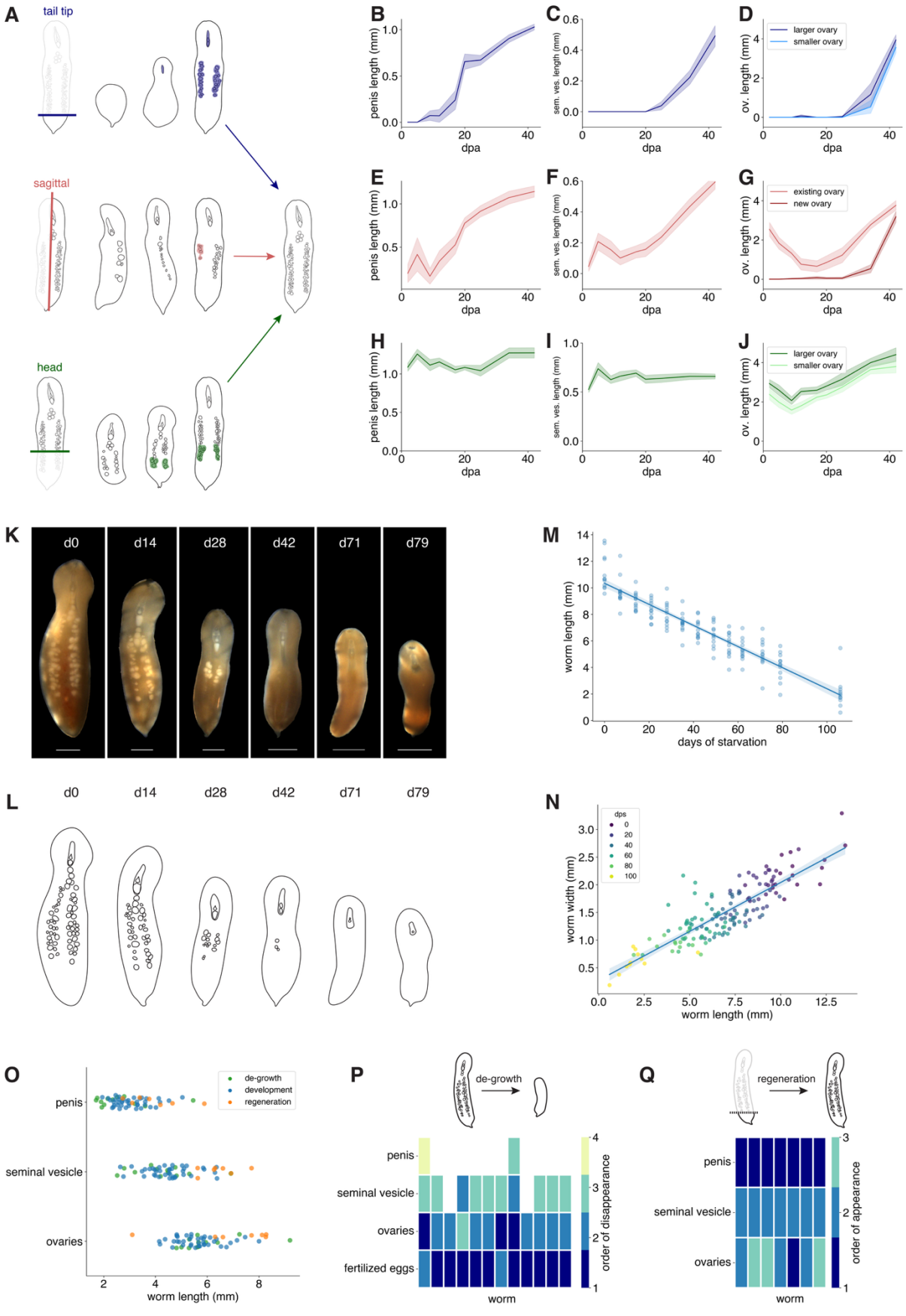
A
tail tip
sagittal
head
B
penis length (mm)
dpa
C
sem. ves. length (mm)
dpa
D
larger ovary
smaller ovary
ov. length (mm)
dpa
E
penis length (mm)
dpa
F
sem. ves. length (mm)
dpa
G
existing ovary
new ovary
ov. length (mm)
dpa
H
penis length (mm)
dpa
I
sem. ves. length (mm)
dpa
J
larger ovary
smaller ovary
ov. length (mm)
dpa
K
d0
d14
d28
d42
d71
d79
M
worm length (mm)
days of starvation
L
d0
d14
d28
d42
d71
d79
N
dps
0
20
40
60
80
100
worm width (mm)
worm length (mm)
O
de-growth
development
regeneration
penis
seminal vesicle
ovaries
worm length (mm)
P
de-growth
penis
seminal vesicle
ovaries
fertilized eggs
order of disappearance
worm
Q
regeneration
penis
seminal vesicle
ovaries
order of appearance
worm

286 **Figure 2: Reproductive organ growth follows similar patterns in different contexts.**
287 (**A**) Schematic of regeneration of the penis, seminal vesicle, and ovaries following three different
288 amputations. Shading indicates the tissue that regenerates. (**B-J**) Growth dynamics of reproductive
289 organs (within column) for each of three amputations (within row). Error bands show SEM. (**K**) Time
290 course of a starving worm undergoing de-growth and step-wise loss of reproductive organs. (**L**)
291 Schematic of reproductive organ degradation as seen in (**K**) over the course of starvation-induced de-
292 growth. (**M**) Worm length decreases over the course of degrowth ($R^2 = 0.85$, $p < 0.0001$). Error band
293 shows 95% confidence interval. (**N**) Worms shrink as they grow; their lengths and widths decrease
294 proportionally ($R^2 = 0.73$, $p < 0.0001$). Error band shows 95% confidence interval. (**O**) Across different
295 growth contexts, reproductive organs appear or disappear at roughly consistent body lengths. Ranking
296 the order in which reproductive structures are lost in worms undergoing de-growth (**P**) and gained in
297 regenerating worms (**Q**) shows that organs are gained and lost in roughly the same order in all growth
298 contexts. The x-axis shows individual worms in these plots. dps = days post onset of starvation. dpa =
299 days post amputation. Scale bars: 1 mm.
300
301
302 **Fine structure of the male reproductive system**
303 To understand the organization of male reproductive structures at high resolution, we visualized
304 them using a combination of histology, immunofluorescence, staining with live dyes, and
305 fluorescence *in situ* hybridization (FISH) (Fig. 3; Fig. S5A). The most anterior part of the male
306 copulatory apparatus is the penis. This structure is difficult to visualize under reflected white
307 illumination (Fig. 1C; Fig. S1A), but can be seen when worms extend it, which we have
308 observed them do both spontaneously and during mating (data not shown). Staining fixed
309 worms with the dye SiR-actin labels the structure clearly, and can be visualized well in smaller
310 adult worms more amenable to confocal microscopy, enabling a high-resolution view of the
311 structure (Fig. 3A-C). Components of the penis can also be seen clearly in histological sections
312 of adult worms (Fig. 3D). These show that the penis contains a bundle of rigid needle-like

structures (referred to as stylets) (Fig. 3E-G, Fig. S5B,C). Our observations of the stylets match the description of sclerotized needles described in other species in the genus and in other studies of *Hofstenia miamia* (Beltagi and Mandura, 1991; Bock, 1923; Corrêa, 1960; Hooge et al., 2007; Steinböck, 1966). The stylets are situated immediately posterior to the base of the penis sheath – a long, conical structure (Fig. 3C; Fig. S5E,F; Video 1). The cavity in the anterior of this sheath has previously been referred to as the 'male antrum' (Beltagi and Mandura, 1991; Bock, 1923; Corrêa, 1960; Hooge et al., 2007; Steinböck, 1966). The base of the sheath is cup-shaped, and is lined with posterior-facing hair-like extensions (Fig. 3G). At its anterior end, it connects to the male gonopore (Fig. 3C). Both the gonopore and the sheath are lined with cilia (Video 1,2), consistent with reports in other hofsteniid species (Beltagi and Mandura, 1991; Bock, 1923; Corrêa, 1960; Hooge et al., 2007; Steinböck, 1966). During mating, the penis stylets are likely pushed anteriorly, through the sheath and out of the male gonopore. This could evert the sheath, resulting in a penis-extension state in which the sheath emerges through the gonopore around the stylet, with the ring of protrusions now near the anterior tip of the penis. It is possible that these protrusions have a sensory function, and could inform fine penis movements during mating. Immunofluorescence with an antibody against FMRFamide (see Methods) revealed a set of cells that resemble neurons encircling the base of the sheath (Fig. S5E). Further studies will be needed to understand how these components regulate copulatory behavior.

Next, we focused on the teardrop-shaped prostatic vesicle, which is situated anterior to the seminal vesicle (Fig. 1C,D) and immediately posterior to the penis stylets (Fig. 3H,I). Our histological studies show that the prostatic vesicle (Fig. S6C-E) is surrounded by glands (Fig. S6F-H). The secretions of this organ are thought to mix with the sperm as it passes through (Faubel, 1983; Hyman, 1951). Unexpectedly, our immunofluorescence experiments also revealed a layer of cells enclosing the prostatic vesicle (Fig. 3I). This layer may be an epithelial

339 tissue most likely associated with the prostatic glands. The interior of the prostatic vesicle
340 contains densely-packed sperm cells (Fig. 3D,I; Fig. S6C-G).
341
342 The seminal vesicle is the posterior-most organ of the male copulatory apparatus (Fig. 3J).
343 Histological staining as well as immunofluorescence staining of the muscle marker
344 Tropomyosin, showed that the seminal vesicle and prostatic vesicle are both encircled by layers
345 of muscle (Fig. S5F; Fig. S6C-H), consistent with previous descriptions (Beltagi and Mandura,
346 1991; Bock, 1923; Corrêa, 1960; Steinböck, 1966). Histological and nuclear staining of the
347 seminal vesicle in adult worms (Fig. 3J-L; Fig. S5F; Fig. S6G,H) reveal that it consists primarily
348 of sperm cells. To confirm this, we dissected the seminal vesicle out of adult worms, and stained
349 it with a nuclear dye. We found that individual cells exited the structure over time, and high-
350 magnification imaging showed that they were indeed sperm cells, each with a ~23μm-long
351 nucleus and a ~22μm-long flagellum (Fig. 3M). During one mating event, we observed a failed
352 attempt at insemination by a worm that resulted in the release of a packet of sperm outside its
353 partner. We recovered this 0.6 mm-long packet of sperm (Fig. S5G) and found that it consisted
354 of cells with the same morphology as those in the seminal vesicle (Fig. S5H), confirming that
355 these are indeed sperm. As an aside, acoel sperm has historically been described as
356 “biflagellate”, intended to mean that sperm cells each contain two axonemes, and this property
357 is thought to be a defining synapomorphic character of acoels (Achatz et al., 2013; Petrov et al.,
358 2004). We show that *H. miamia* sperm have a single flagellum, and suggest that the axonemal
359 properties of the flagellum may be more accurate taxonomic characters than external flagellar
360 morphology.
361
362 Next, we sought to identify the testes (the organs of sperm production). Consistent with previous
363 observations (Beltagi and Mandura, 1991; Bock, 1923; Corrêa, 1960; Hooge et al., 2007;
364 Steinböck, 1966), nuclear staining and histological studies of adult worms revealed dense

clusters of sperm in the anterior parenchyma, wrapping around the worm's pharynx (Fig. 3N-U). Tropomyosin labeling showed that the testes are embedded within layers of muscle (Fig. S5I,J). Next, inspecting germline markers identified in previous single-cell RNA sequencing data (Hulett et al., 2023), we identified one likely to label testes: the gene *pa1b3-2*. FISH for *pa1b3-2* reveals that this gene does indeed specifically label testes, and that its expression coincides well with the dense cellular clusters visible through nuclear staining (Fig. S7A,B).

Finally, we studied the development of the male reproductive system, using confocal microscopy to visualize the maturation of its components at high resolution. Hatchling worms do not possess any visible reproductive structures. Actin staining reveals that, within the copulatory apparatus, the sheath and stylets emerge first, followed by a gradually-inflating prostatic vesicle (Fig. 4A). The hair-like extensions of the sheath grow and become more conspicuous over time (Fig. 4A). We used two methods to visualize testes maturation. First, reasoning that nuclear staining may not allow us to visualize testes at the earliest developmental stages, we performed FISH to detect mRNA for *pa1b3-2* in juvenile worms of various sizes. In the smallest worms (i.e. ~<2 mm), there was no expression (Fig. 4B-C). In larger, reproductively immature worms, we detected expression of *pa1b3-2* in two lateral clusters that expanded slightly along the anterior-posterior axis as development progressed (Fig. 4B-C). Since adult testes are a single cylindrical structure that wraps around the pharynx, this early developmental pattern suggests that the two lateral structures must grow along the dorso-ventral and medio-lateral axes until they meet in the middle. Second, to test this hypothesis, we performed nuclear staining on transverse sections of worms across a broader section of development (Fig. 4D; Fig. S7C). In small worms, the testes are lateralized and do not meet on the dorsal surface. In larger worms, these lateral regions have expanded across the dorsal surface of the worm to form a single apparently-continuous region (Fig. 4E). Many acoel species are thought to have paired, lateral testes (Table S1), a feature of taxonomic importance (Jondelius et al., 2011). While juvenile *H. miamia*

391 have paired testes, these organs morph into a single cylindrical structure in the transition to
392 adulthood. As lab-reared worms can be substantially larger than those found in the wild, these
393 results raise the possibility that other acoels may undergo similar morphological changes during
394 development.
395
396 Together, our data provide a high-resolution view of *H. miamia's* elaborate male reproductive
397 morphology. Consistent with our quantitative data, we find that this morphology emerges in a
398 stereotyped developmental sequence during the transition to adulthood in which the penis
399 sheath develops first, followed by nascent testes, the stylets, and the membrane-like structure
400 enveloping the prostatic vesicle. Sperm, presumably from the testes, then travels to the
401 prostatic vesicle. Over time, as all structures grow, the hair-like projections on the back of the
402 sheath become more prominent, the testes extend both along the anterior-posterior axis and
403 dorsally to wrap around the head, and sperm cells fill the seminal vesicle. The prostatic and
404 seminal vesicles appear to be surrounded by muscle, epithelia, and gland cells. Our histological
405 sections suggest that at least in adult worms, sperm cells may enter the seminal vesicle and
406 travel forwards into the prostatic vesicle. We do not yet understand how this occurs in juvenile
407 worms, how sperm cells navigate to these vesicles from their varied points of origin, or how they
408 are hypodermically injected during mating.
409

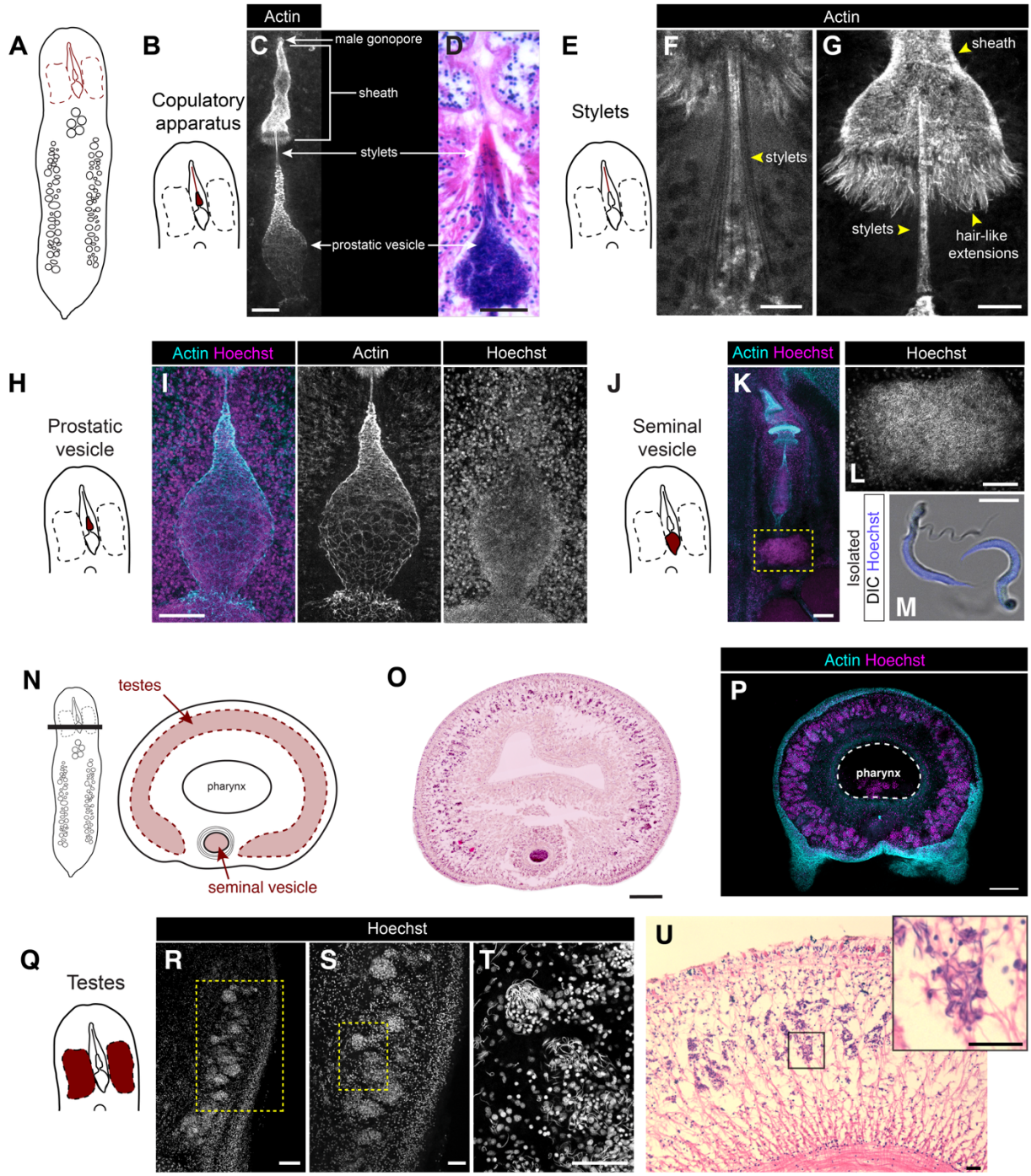

410

411 **Figure 3: Male reproductive anatomy.** (**A**) A schematized view of the ventral surface of the worm with

412 male reproductive structures highlighted in red. (**B**) Schematic of male reproductive structures with the

413 copulatory apparatus (excluding the seminal vesicle) highlighted. (**C**) Labeling with an actin dye (white)

414 labels the male gonopore, sheath, penis stylet, and prostatic vesicle. (**D**) A histological section also

415 reveals these organs. (**E**) Schematic of the male reproductive system, with the penis stylet highlighted. (**F**)

The stylets are a bundle of needles labeled by actin. (**G**) The posterior of the penis sheath terminates in a ring of hair-like projections, also labeled by actin. (**H**) Schematic of the male copulatory apparatus, with the prostatic vesicle highlighted. (**I**) Actin staining with a nuclear label (Hoechst) shows that the prostatic vesicle is enveloped by a thin epithelium-like layer, and contains densely packed sperm. (**J**) Schematic of the male copulatory apparatus, with the seminal vesicle highlighted. (**K**) The morphology of the copulatory apparatus in mature, adult worms is similar to that of early adults (previous panels). (**L**) The seminal vesicle of this adult worm contains densely-packed sperm. (**M**) Dissecting out an adult seminal vesicle allows labeling of individual sperm cells, showing their distinctive morphology. (**N**) Schematic of a transverse view of an adult worm's anterior, showing the relative organization of the seminal vesicle and testes. (**O**) Transverse sections show that testes appear as a continuous structure that spans the dorsal surface of the worm. (**P**) The testes extend through the dorso-ventral axis of the worm and wrap around the head. The pharynx (labeled and circled with a dotted line) contains residual food. (**Q**) Schematic of the male copulatory apparatus, with the testes highlighted. (**R-T**) Nuclear staining on an adult worm, cut sagittally, reveals the testes, which contains dense bundles of sperm organized around clusters of cells in the parenchyma. (**U**) Histological sections confirm this organization of the testes. Scale bars: 20μm (C, U), 10μm (F-G, M), 50μm (D,I,S, T), 100μm (K,L,R), 200μm (O, P).

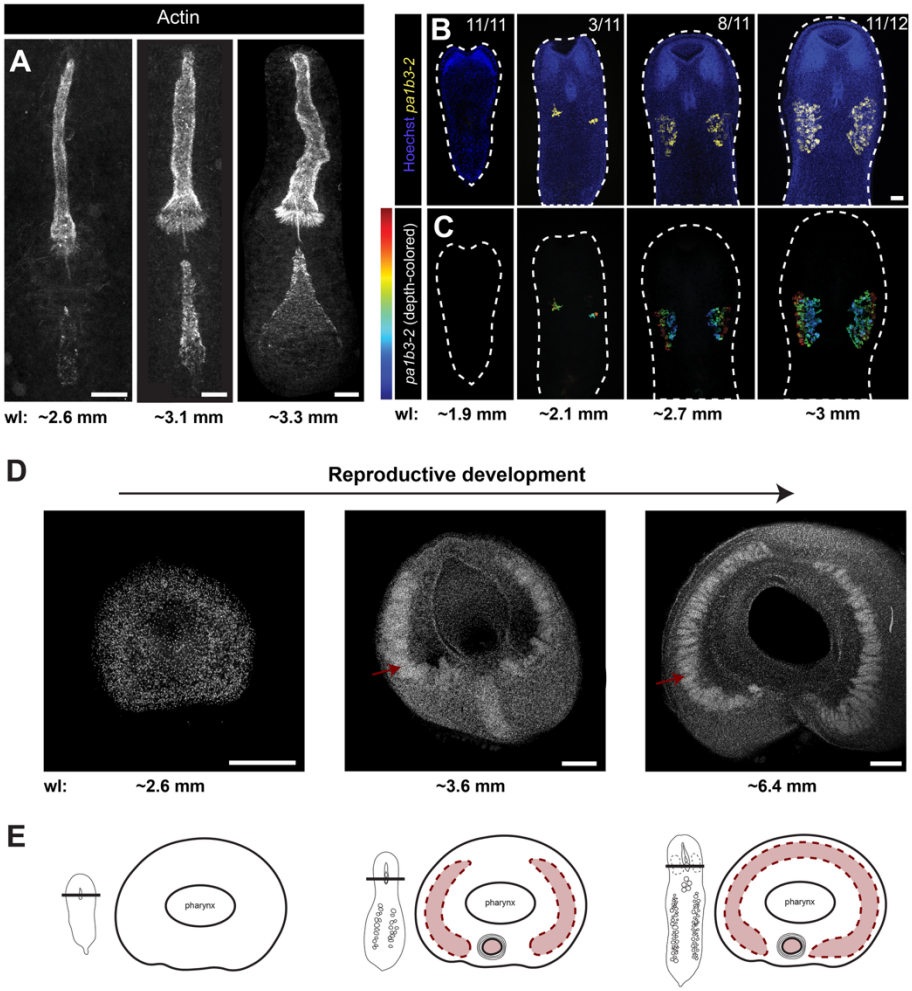

433

434 **Figure 4: Stepwise emergence of components of the male reproductive system.** (**A**) Actin-dye
435 labeling shows how the male reproductive system changes over the course of post-embryonic
436 development (shown here from left to right). The sheath and stylet emerge first, followed by the
437 appearance of the prostatic vesicle. (**B**) FISH for the male germline marker *pa1b3-2* results in two regions
438 of ventrolateral expression that extend along the dorsal-ventral axis to different depths. Images are
439 organized by pseudo-time: from least-developed (and smallest) on the left, to most-developed (and
440 largest) on the right. Panels in (**C**) show depth-coloration, showing that the testes extend through the
441 dorso-ventral axis. (**D**) Cross-sections of worms at different points in reproductive development stained
442 with nuclear dye show that testes grow towards the dorsal surface and eventually meet to form one
443 continuous structure. (**E**) Cartoon schematic of cross-sections shown in (**D**). Scale bars: 20μm (A), 100μm
444 (B, C), 200μm (D). Estimated worm lengths (wl) are noted under each panel.

445

446 **Fine structure of the female reproductive system**

447 As observed through imaging of adult worms using a stereo microscope, the female
448 reproductive system in *H. miamia* consists of two lateral ovaries running longitudinally along
449 both sides of the body, and one medial cluster of mature eggs located posterior to the pharynx
450 (Fig. 5A-C). To visualize the structure of the ovaries, we used FISH to label mRNA of a
451 previously-identified germline marker: *cgnl1-2* (Hulett et al., 2023). We found that this gene
452 specifically labeled the oocytes (Fig. 5D). Moreover, immunostaining with a custom antibody
453 against Piwi-1 (typically a stem cell and germline marker) also labeled the ovaries (Fig. 5E).
454 Unlike in many other organisms where *piwi* homologs are expressed in male gonad tissue
455 (Deng and Lin, 2002; Gonzalez et al., 2015; Jehn et al., 2018; Kuramochi-Miyagawa et al.,
456 2004; Miramón-Puértolas et al., 2024), we did not detect Piwi-1 expression in *H. miamia* testes.
457 Possible explanations include potential low expression of Piwi-1, the use of other Piwi proteins
458 in spermatogenesis, or that male germline progenitors (which could express Piwi-1) may not be
459 co-located with maturing sperm in the testes. We were also able to visualize the ovaries in
460 histological sections (Fig. 5C). These methods, together with our earlier images of ovaries at
461 different worm ages, showed that oocytes are not organized by maturity within the ovary (Fig.
462 S8A). We did not detect a membrane or lining that envelopes the ovaries. This is consistent with
463 previous work that suggests that acoels lack true ovaries *sensu stricto*: oocytes appear and
464 develop within the parenchymal tissue without a specialized membrane that forms a discrete
465 organ (Eckelbarger and Hodgson, 2021; Rieger et al., 1991; Schmidt-Rhaesa, 2007).

466

467 Oocytes in *Hofstenia* are surrounded by a layer of follicular cells, which are thought to provide
468 nutrition and secrete the eggshell (Bock, 1923; Rieger et al., 1991). We visualized this cell layer
469 with immunofluorescence and histology and found that it was consistently present around every
470 oocyte in the ovaries irrespective of their developmental stage (Fig. 5F-G; Fig. S8B-D). We

observed that many follicle cells have very large nuclei, perhaps the result of the fusion of neighboring cells (Fig. 5G; Fig. S8B-C). We also found clusters of sperm in the layer of follicular cells surrounding maturing oocytes of a variety of developmental stages (Fig. 5F,G, insets), consistent with Bock's (1923) proposal that the follicle may 'trap' sperm and control the fertilization of maturing oocytes. All oocytes contained a granular substance primarily distributed peripherally, and a germinal vesicle occupying a substantial portion of the oocyte (Fig. 5H-J). A germinal vesicle, a nucleus arrested in prophase I of meiosis, is a feature of oocytes in most animals (Grossman et al., 2017; Herlands and Maul, 1994; Liu et al., 2006; Munro et al., 2023). It is broken down during oogenesis or after fertilization (Falleni & Gremigni, 1990; Sagata, 1996). The presence of a germinal vesicle in the oocytes in *H. miamia*'s ovaries suggests that these oocytes are unfertilized. It is likely that oocytes mature in the ovaries, the germinal vesicle then breaks down, following which oocytes are fertilized. These mature, fertilized eggs may then travel from the ovary to the central cavity prior to being laid.

We could not determine conclusively where or when fertilization happens, or where the egg capsule (chorion) is produced. However, the spatial organization of the female reproductive system suggests that an oocyte must mature, become fertilized, and then be transported to the cavity behind the pharynx. Our internal examinations did not identify any oviducts, canals or additional structures that could facilitate this migration from the ovaries to the medial cluster. How eggs are transported thus remains unknown.

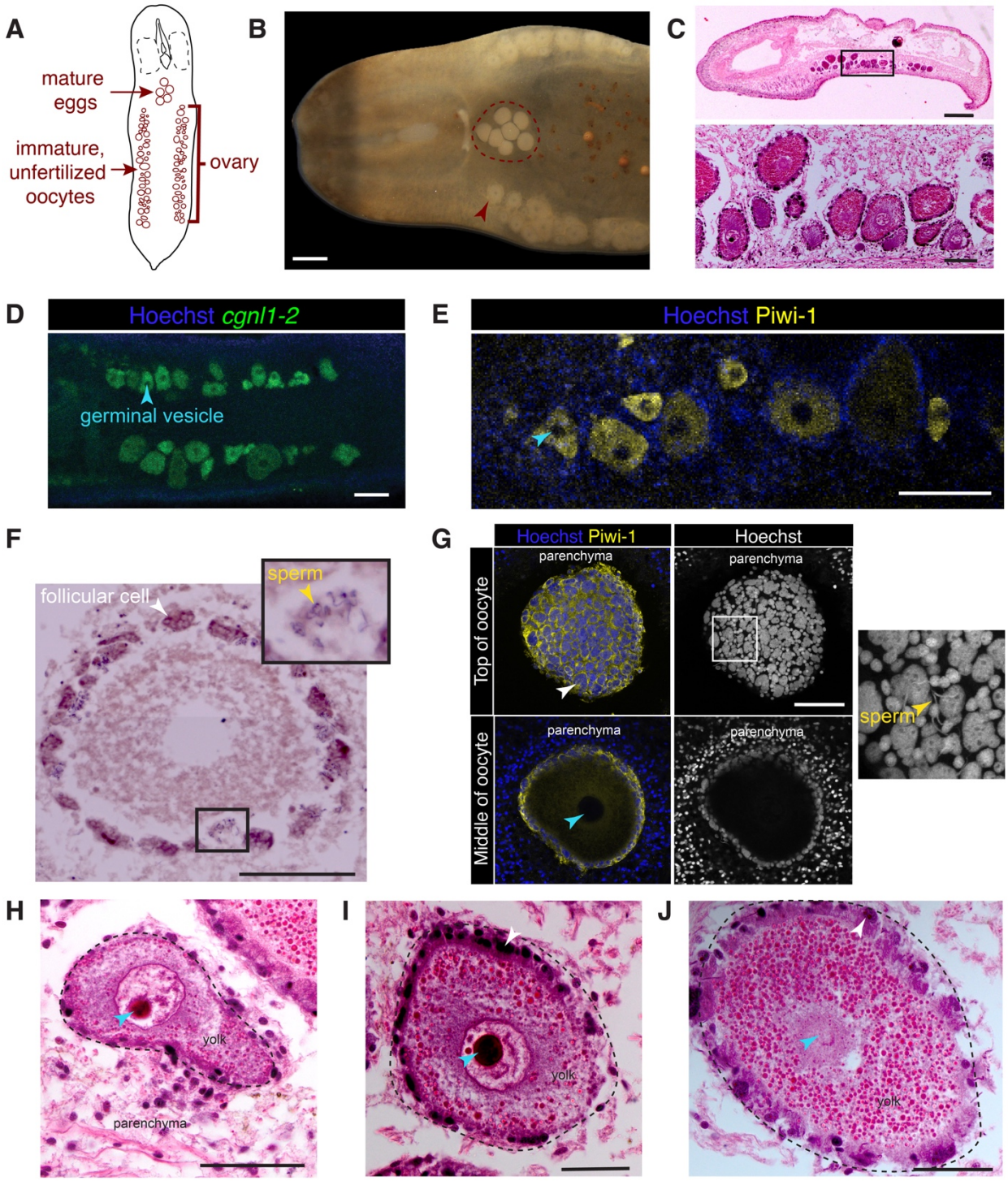

Figure 5: Female reproductive anatomy. (**A**) A schematized view of the ventral surface of the worm with female reproductive structures highlighted. (**B**) Eggs near the pharynx of the worm (within the red circle) are fertilized and mature while oocytes in ovaries (red arrow) are immature or unfertilized, with a visible germinal vesicle. (**C**) A sagittal histological section shows that the ovaries contain oocytes of varied

497 size and maturity embedded in the parenchyma. (**D**) FISH shows that *cgnl1-2* labels immature oocytes in
498 the ovaries. (**E**) Oocytes in ovaries are also labeled by a Piwi-1 antibody. (**F**) A histological transverse
499 section of an immature oocyte encircled by follicular cells. Inset: sperm cells appear to be trapped in the
500 follicle. (**G**) Piwi-1 immunofluorescence confirms the organization of follicular cells, and nuclear staining
501 sometimes identifies sperm apparently trapped in its surface (inset). Histology also shows that immature
502 oocytes may have irregular shapes (**H**), contain a germinal vesicle (**H,I**), and possess an abundance of
503 (likely yolk) granules (**I,J**). Blue arrows label germinal vesicles in all relevant panels; yellow arrows label
504 sperm; white arrows label follicular cells. Scale bars: 100μm (B, C (inset), D-F), 500μm (C), 50μm (G, H-
505 J)
506
507 **Egg-laying behavior**
508 Egg laying has only been directly observed a few times in acoels, mostly in species within the
509 Convolutidae (Costello and Costello, 1939; Gardiner, 1898). From these observations, acoels
510 are known to lay eggs through the female gonopore if present (Gardiner, 1898), a mode of egg
511 laying used by many platyhelminths (Tong and Ong, 2020), or through breaks in the body wall
512 (Apelt, 1969; Costello and Costello, 1939). It has also been suggested that acoels could lay
513 eggs through the mouth; however, direct observation of such egg laying has been challenging
514 (Apelt, 1969; Costello and Costello, 1939; Watzin, 1984).
515
516 Previous authors have speculated that *H. miamia* lay eggs through breaks in the body wall, or
517 perhaps partially through the mouth, but egg laying was not observed (Bock, 1923; Steinböck,
518 1966). To observe how worms lay eggs, we isolated gravid adult worms and filmed them from
519 underneath for a 24 hour period. 3 worms laid a total of 25 eggs in these conditions. We found
520 that worms exclusively laid eggs through their mouths, one at a time, in events typically lasting
521 less than 2 minutes each (Fig. 6A,B; Video 3; Fig. S9A). During this event, the worm performs a
522 series of muscle contractions to transfer a single egg from the ventral medial cavity of fertilized
523 eggs into the pharynx, and then applies further muscle contractions from posterior to anterior to

move the egg to the mouth. The worm then places each egg on the substrate with its mouth, likely secreting mucus to attach the egg to the substrate (Fig. 6A,B; Video 3). Observations from these videos, as well as of egg clutches in our culturing tanks, show that worms can either deposit a single egg in one location or lay eggs in one or more clutches.

To understand the temporal dynamics of egg-laying in *H. miamia*, we then quantified the time course of egg-laying in several contexts. We found that adult worms with previous access to mates, once isolated, continued laying eggs for over a month (Fig. 6C). Juvenile worms reared to adulthood in isolation laid a single burst of eggs (Fig. 6D), multiple months after first being isolated (although the timing of this burst may depend on rearing conditions and the health of the worms). Consistent with our finding that worms reared entirely in isolation can lay eggs (Fig. 1L,M), this burst of egg laying is also likely the result of a selfing event in which the worms fertilize their own eggs, or possibly the result of a form of parthenogenesis allowing the activation of unfertilized eggs. We also allowed virgin worms to mate once, in controlled conditions, and subsequently isolated them. These mated and inseminated worms laid eggs for over three months after a single mating (Fig. 6E). One possibility is that these eggs are the result of self-fertilization; however, selfing produces a single burst of egg-laying after isolation (Fig. 6D). Instead, these data (considered with our observations of adult ovaries (Fig. 5F,G)) suggest that sperm received during mating may be stored in follicular cells for several months.

Next, we asked how much control the worms had over their egg laying. To test whether worms choose specific locations to lay eggs, we quantified the spatial positions of eggs laid in their culturing tanks. We found that worms have a strong preference for laying eggs on the walls of their tanks, rather than on the floor (Fig. 6F). Eggs laid on walls are preferentially laid close to the water line (Fig. 6G, Fig. S9B). This preference is not simply because the worms lay eggs where they are: we observed that worms spend the majority of their time on the floors of their

550 tanks, and seem to glide up the walls specifically to lay eggs (Fig. S9C). These spatial
551 preferences do not seem affected by food availability: when deprived of food, egg laying still
552 primarily occurs on the walls of culture tanks (Fig. S9D). These data suggest that worms make
553 active substrate choices for egg laying.
554
555 We also observed that worms lay 49% of their eggs in clutches. Individual worms can produce
556 these clutches (Video 3). Clutch sizes are often small (Fig. S9E), but the largest can contain
557 over 30 eggs deposited within a 3-4 day window in culture tanks containing 20-50 worms (Fig.
558 6H, Fig. S9E). The vast majority of individual worms lay fewer than 10 eggs in a 3-4 day period
559 (Fig. S9F), suggesting that some clutches may be communal. Indeed, in other culturing
560 conditions with large groups of worms, clutch size often exceeds 140 eggs (Fig. 6I). To test
561 whether worms lay eggs in communal clutches, we allowed worms to lay eggs in tanks for 3
562 days. We then swapped worms between tanks (or, for control tanks, we swapped worms and
563 removed old eggs). We asked how worms interacted with egg clutches laid in the first 3-4 days,
564 and found that many new eggs were laid in pre-existing clutches (Fig. 6J, Fig. S9G). Worms
565 added new eggs to 42 percent of old egg clutches. This shows that worms frequently lay eggs in
566 communal egg clutches.
567
568 Finally, we asked whether worms withhold eggs in suboptimal environments. Our observations
569 (see Fig. 2K-L) suggested that worms are physiologically resilient to food stress. We therefore
570 conducted an experiment with a set of worms, half of which were deprived of food for one
571 feeding period (3-4 days). The other half were fed normally during this period. We found that
572 food-deprived worms laid significantly fewer eggs during this period (Fig. 6K). We hypothesized
573 that this reduction in egg-laying was because the worms were actively withholding their eggs in
574 the absence of food. Next, we repeated this experiment, first depriving some worms of food and
575 subsequently feeding them. After food-deprived worms were given food, they laid an excess of

576 eggs (Fig. 6L), showing that the worms withhold egg-laying in food-limited environments. More
577 generally, these data show that *H. miamia* assess their environments to decide when and where
578 to lay eggs.
579

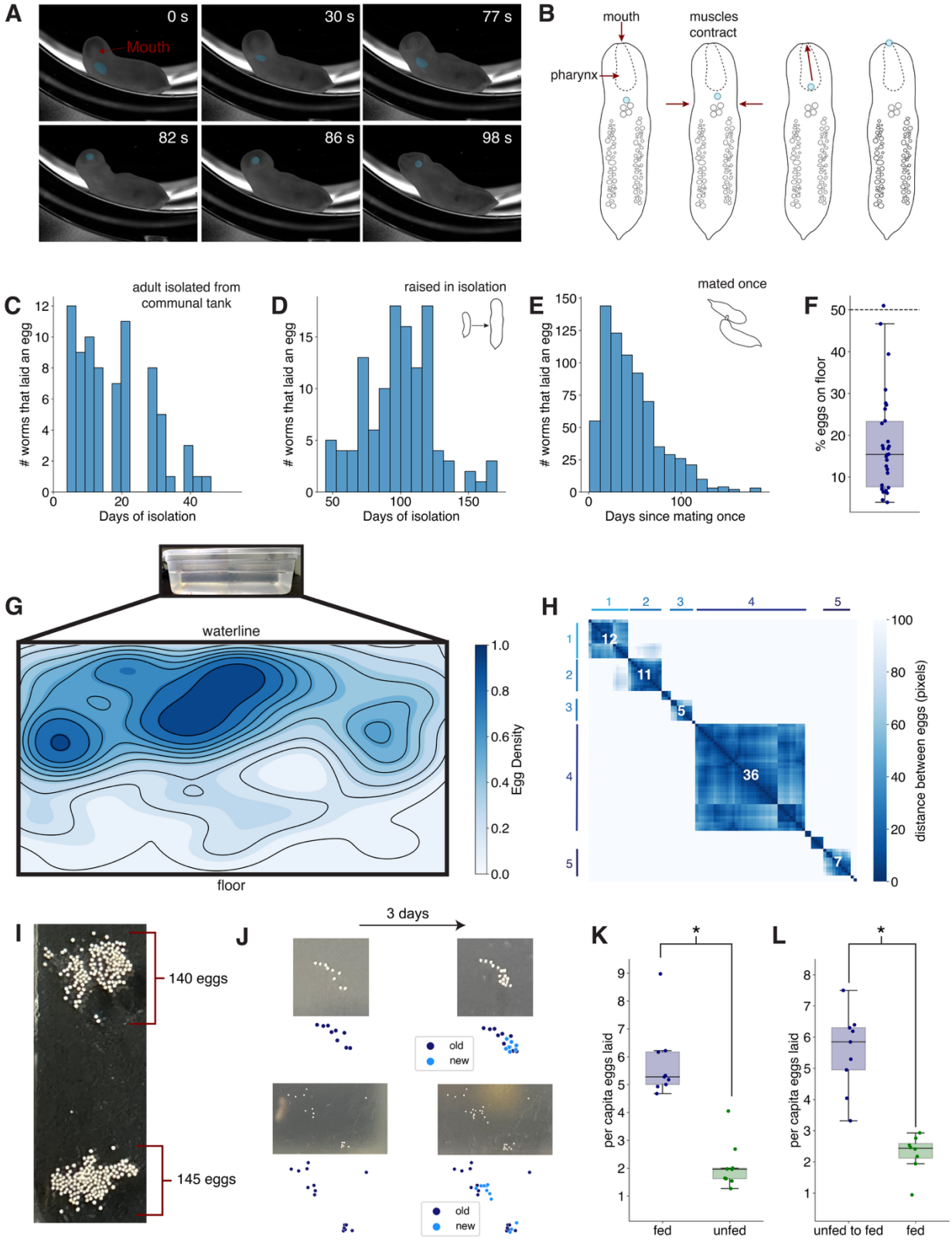
A
0 s
30 s
77 s
82 s
86 s
98 s
Mouth
B
mouth
muscles contract
pharynx
C
adult isolated from communal tank
worms that laid an egg
Days of isolation
D
raised in isolation
worms that laid an egg
Days of isolation
E
mated once
worms that laid an egg
Days since mating once
F
% eggs on floor
G
waterline
floor
Egg Density
H
distance between eggs (pixels)
I
140 eggs
145 eggs
J
3 days
old
new
K
per capita eggs laid
fed
unfed
L
per capita eggs laid
unfed to fed
fed

580

Figure 6: *H. miamia* lays eggs through its mouth and exhibits environmental preferences in egg laying. (**A**) Sequence of images from a video of egg-laying through the mouth. Eggs in the pharynx and emerging through the mouth are shaded blue. (**B**) Schematic showing presumed process of embryo traveling from the cavity beneath the pharynx to the pharynx and then out through the mouth. (**C**) Histogram showing the timing of eggs laid by adult worms living in communal tanks and then isolated. (**D**) Histogram showing the timing of eggs laid by worms that undergo reproductive development in isolation and then self-fertilize. (**E**) Histogram showing the timing of eggs laid by worms that are allowed to mate once. (**F**) Scatterplot of the percentage of eggs found on the floor of communal tanks ($n = 30$). This is significantly different from the expected percentage of eggs based on tank surface area (t-test $p < 0.0001$). (**G**) Kernel density estimate of egg locations on a subset of tank surfaces with similar dimensions ($n = 2144$ eggs). (**H**) Distance matrix of egg coordinates, with density-based spatial clustering, from a representative tank surface shows that eggs are often laid in clutches. Number of eggs in a clutch is shown in white; cluster identity is shown on the x and y axes. (**I**) In some culturing conditions, worms lay clutches of up to 145 eggs. (**J**) New worms add eggs to pre-existing clutches laid by other worms. (**K**) Worms that are unfed for 4 days lay fewer eggs than fed worms ($n = 9$ tanks, t-test $p < 0.0001$). (**L**) Unfed worms that are subsequently fed lay more eggs than worms that are continuously fed ($n \geq 8$ tanks, t-test $p < 0.0001$).

Discussion

Our work describes the reproductive life history of an acoel across its life cycle (Fig. 7A). We reveal many new facets of acoel biology, describe the structure and dynamics of growth, regeneration, and egg-laying behavior, and establish a foundation for the experimental study of reproductive biology in acoels. Below, we discuss the significance of our findings for reproductive development, behavior, and the evolution of life history strategies.

Reproductive development and regeneration

Little is known about the development or regeneration of reproductive structures in acoels. Our data show that in *H. miamia*, reproductive structures develop and regenerate in a stereotyped sequence, with male organs appearing before female ones. During starvation-induced de-growth, these organs degenerate in the opposite sequence. This stereotypy is unexpected and may not be a universal feature of acoels: sparse data from three other acoel species, *Solenofilomorpha funilis* (Crezée, 1975), *Otocelis luteola* (Kozloff, 2000a) and *Aphanostoma pulchra* (Perea-Atienza et al., 2013), indicate that these species do not exhibit identical sequences. The stereotypy we observe is consistent with the idea that a single, size-associated program regulates reproductive organ development in *H. miamia*, and that it may be deployed in a variety of growth contexts.

Our results also show that *H. miamia* is capable of regenerating all reproductive structures from a variety of initial tissue configurations. The trajectories toward organ replacement vary based on this initial state, and reveal important features of the regenerative process. For instance, we found that worms missing their sagittal halves or their tails first shrink in size before re-growing. This may be in part because the early stages of wound closure and regeneration require the reorganization of existing tissues. In any case, this reduction in body size is associated with disproportionate reductions in reproductive organ size, demonstrating active tissue destruction

mechanisms, possibly mediated by apoptotic processes similar to those reported in other regenerative species (Ballarin et al., 2008; Pellettieri et al., 2010; Rychel and Swalla, 2008). In addition, we found that the two ovaries within a worm grow in a significantly correlated manner, and after sagittal amputation, the missing ovary grows disproportionately to regenerate symmetry. In principle, such bilateral symmetry could be achieved passively, without any feedback (Reddien, 2018). However, the strong within-worm correlation, even after controlling for body size, suggests that there is either organism-specific coordination of growth or death rates, or more likely a feedback process that ensures bilateral symmetry.

In many animal lineages such as arthropods, vertebrates, planarians, and nematodes, organs typically grow symmetrically, and scale with body size (Boulan and Léopold, 2021; Ko et al., 2024; Uppaluri and Brangwynne, 2015; Wolpert, 2010). The mechanisms underlying this coordinated, scaled growth are not fully understood, and may vary across tissues and species. For instance, some vertebrate tissues appear to grow using cell-intrinsic programs; others – and many insect tissues – appear to rely on central coordinating mechanisms that read signals of growth from the circulation or from unknown sources (Allard and Tabin, 2009; Boulan and Léopold, 2021; Harris et al., 2021; Trible and Kronauer, 2017; Vallejo et al., 2015; Wolpert, 2010). How different organs ensure appropriate, coordinated scaling remains poorly understood. We find that *H. miamia* must also solve this problem: their reproductive organs scale with body size during development, regeneration, and de-growth, and an active coordination mechanism ensures that the ovaries return to symmetry after perturbation. How do tissues across the body ‘read’ the same indicators of size, and how is their growth coordinated? Our work establishes a foundation for the experimental study of these and other developmental phenomena.

Egg-laying physiology and behavior

Few acoels have been directly observed laying eggs (Costello and Costello, 1939; Gardiner, 1895; Watzin, 1984). We find that *H. miamia* lays fertilized eggs through its mouth: a mode of egg-laying not observed in other animals. This unusual behavior raises multiple questions. First, where in the animal does fertilization occur? Our observations suggest that follicular cells surrounding immature oocytes may act as a selective barrier to sperm, preventing many sperm cells from reaching the oocyte, a function suggested by Bock (1923). Additionally, given that *H. miamia* can lay eggs for months after a single mating despite lacking a seminal bursa, it is likely that the follicular cells function as a sperm storage organ. Second, we find that *H. miamia* appears capable of self-fertilization as it can lay eggs without mating. While some acoels are capable of asexual reproduction through fissioning and budding (Åkesson et al., 2001; Ax and Schulz, 1959; du Bois-Reymond Marcus, 1955; Hanson, 1960; Ishikawa and Yamasu, 1992; Zabotin and Evtugyn, 2021), self-fertilization has not been reported previously. How does sperm travel to the ovaries? It is likely that sperm cells migrate posteriorly from the testes towards the ovaries in isolated worms, and from arbitrary body regions towards the ovaries after mating. In addition, sperm must travel from all regions of the testes to the seminal and prostatic vesicles. Whether they use chemical cues to navigate towards oocytes and these vesicles, and the mechanics of this process, remain unknown. Third, how do mature eggs travel from the lateral ovaries to the medial cavity, and how are the eggs in this cavity physically loaded into the pharynx? Our anatomical observations have so far failed to reveal obvious oviducts, or other tube-like structures that could facilitate movement of eggs into the pharynx. The only known opening at the posterior of the pharynx is the pharyngeal sphincter that allows food to pass into the gut. We therefore speculate that eggs travel through the gut to the medial cavity, which may simply be a pocket within the gut. Eggs may then be moved into the pharynx through a form of reverse peristalsis (and observation of the worm prior to egg-laying shows waves of muscle contraction proceeding posterior-to-anterior as each egg is loaded into the pharynx).

676 We also find that *H. miamia* appears to make active choices about when and where to lay
677 fertilized eggs. *H. miamia* has clear spatial preferences for egg-laying in our culture chambers.
678 Worms often lay eggs in communal clutches, sometimes adding to another worm's clutch. They
679 also have environmental preferences, withholding egg-laying when deprived of food and then
680 laying these eggs once food becomes available. Together, these results show that *H. miamia*
681 surveys its environment and then integrates this assessment into whether – and where – it is
682 suitable to lay an egg. More generally, the existence of communal egg clutches raises the
683 possibility that acoels may have a rich and unexplored social repertoire.
684
685 **Evolution of reproductive strategies within acoels**
686 Placed in a comparative context, our description of *H. miamia*'s reproductive life history reveals
687 that acoels and their sister lineage, the nemertodermatids, display a striking diversity of
688 reproductive morphologies, and likely a corresponding diversity in reproductive behavior (Fig.
689 7B). This diversity reveals correlated suites of reproductive traits that suggest a small number of
690 life history strategies. For instance, the presence of a bursa and female gonopore are
691 associated with a muscular penis, suggestive of cooperative, genital-handshake style mating.
692 The absence of a bursa and female gonopore are associated with a needle-laden penis,
693 suggestive of competitive, hypodermic-insemination style mating. Comparative work in the
694 distantly-related platyhelminth flatworms shows that these anatomical and behavioral traits
695 indeed coevolve similarly (Brand et al., 2022a, 2022b), in accordance with social evolutionary
696 theory on sexual conflict (Charnov, 1979; Michiels and Newman, 1998; Ramm et al., 2015).
697 Within the genus *Macrostomum*, a competitive hypodermic insemination syndrome has evolved
698 at least 14 times from ancestral cooperative, reciprocal insemination (Brand et al., 2022a,
699 2022b). This syndrome involves the correlated evolution of a sharpened penis, a simplified
700 female sperm-receiving organ, sperm cells lacking bristles and other adaptations for post-
701 copulatory sexual conflict, and associated behavioral changes (Brand et al., 2022a, 2022b,

2022c; Schärer et al., 2014, 2011). Whether similar anatomical associations truly predict mating strategies in acoels remains unknown. In addition, the variability of some morphological features does not obviously fit this pattern of cooperative vs. competitive reproductive strategies. For example, the relative locations of the testes and ovaries is highly variable, as is the number of bursal nozzles, suggesting that there may be further evolutionary patterns awaiting explanation. Our work establishes an approach to study reproductive anatomy and behavior in a model acoel. This approach can be applied to many other acoel species. Given their rich diversity, acoels are a promising clade in which to study the evolution of reproductive strategies, and in which to test the generality of theories of sexual conflict.

Conclusion

These findings establish foundational knowledge of anatomical, physiological, and behavioral elements of *H. miamia*'s reproductive life history. This enables future work on the molecular genetics of reproductive organ development and regeneration, on the physiological processes involved in egg maturation and oviposition, and on the neuroscience of reproductive behavior.

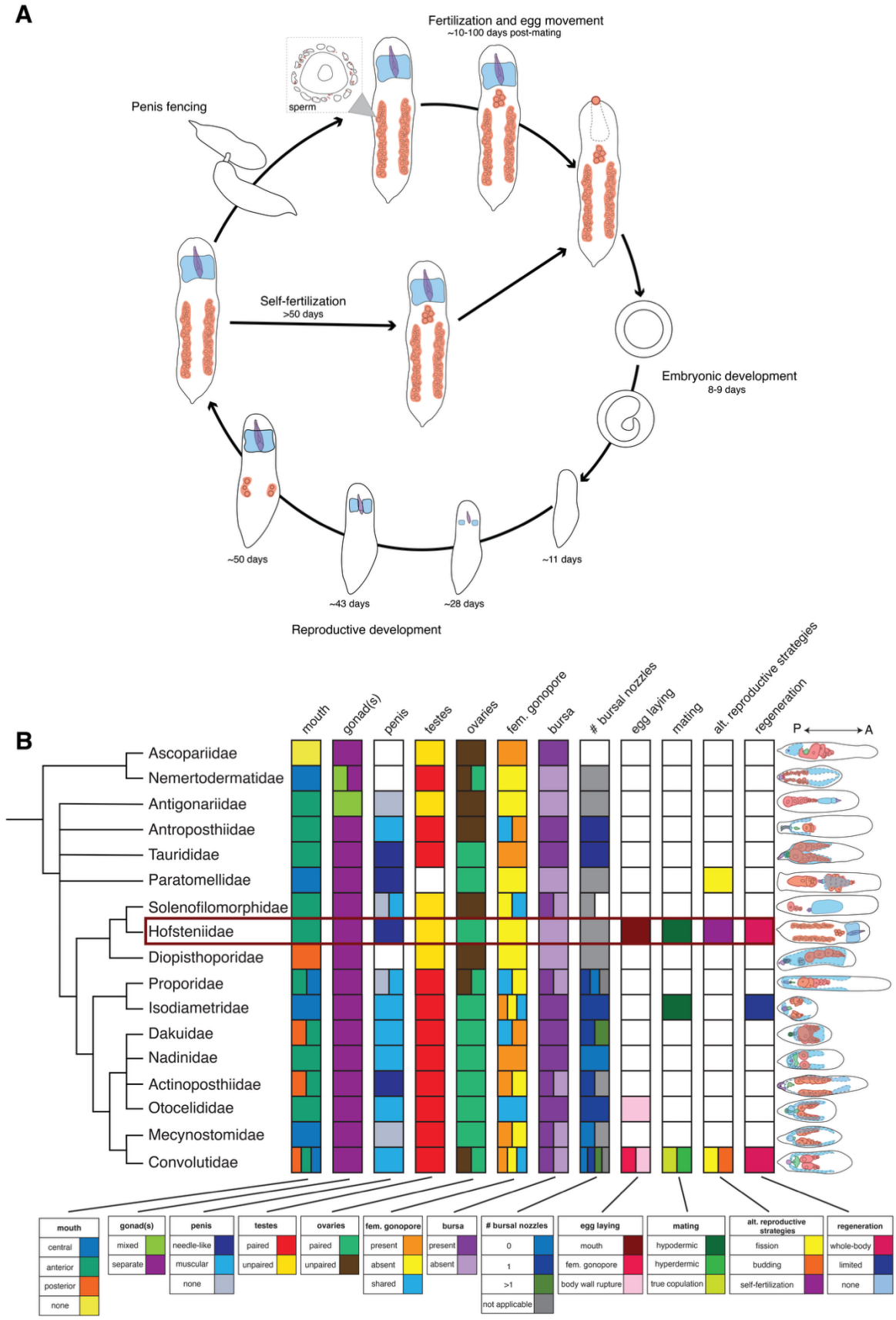
A
Fertilization and egg movement
~10-100 days post-mating
sperm
Penis fencing
Self-fertilization
>50 days
Embryonic development
8-9 days
~11 days
~28 days
~43 days
~50 days
Reproductive development
B
mouth
gonad(s)
penis
testes
ovaries
fem. gonopore
bursa
bursal nozzles
egg laying
mating
alt. reproductive strategies
regeneration
P
A
Ascopariidae
Nemertodermatidae
Antigonariidae
Antroposthiidae
Tauriididae
Paratomellidae
Solenofilomorphidae
Hofsteniidae
Diopisthoporidae
Proporidae
Isodiametridae
Dakuidae
Nadinidae
Actinoposthiidae
Otocelididae
Mecynostomidae
Convolutidae
mouth
central
anterior
posterior
none
gonad(s)
mixed
separate
penis
needle-like
muscular
none
testes
paired
unpaired
ovaries
paired
unpaired
fem. gonopore
present
absent
shared
bursa
present
absent
bursal nozzles
0
1
>1
not applicable
egg laying
mouth
fem. gonopore
body wall rupture
mating
hypodermic
hyperdermic
true copulation
alt. reproductive strategies
fission
budding
self-fertilization
regeneration
whole-body
limited
none

718

Figure 7: Reproductive life histories in Acoelomorpha. (A) The life cycle of *Hofstenia miamia*, with major reproductive events displayed. **(B)** Family-level phylogeny of Acoelomorpha (Nemertodermatida, Acoela) showing anatomical and reproductive life history traits (Table S1): position of the mouth, whether gonads are mixed or separated by sex, penis type, paired or unpaired testes, paired or unpaired ovaries, presence or absence of a female gonopore, presence or absence of a seminal bursa, the number of associated bursal nozzles, egg-laying mode, mode of sexual reproduction, alternative reproductive strategies, and regenerative capacity (see Table S4 for definitions of terms and categories). Schematic diagram of the reproductive anatomy of representative species from each family within Acoelomorpha with specific structures colored: male copulatory organ (purple), sperm in testes and/or seminal vesicle (blue), oocytes (red), female or shared gonopore and/or bursa (green). (Table S1). White boxes represent unknown phenotypic states, and in the case of asexual reproduction, its possible absence. Phenotypic classifications are from (Achatz and Hooge, 2006; Apelt, 1969; Bailly et al., 2014; Beltagi and Mandura, 1991; Bock, 1923; Boone et al., 2011; Bush, 1975; Costello and Costello, 1939, 1938; Crezee, 1978; Dörjes, 1968, 1966; Faubel, 1976, 1974; Faubel and Cameron, 2001; Gardiner, 1895; Grae and Kozloff, 1999; Hooge, 2003; Hooge et al., 2007; Hooge and Smith, 2004; Hyman, 1937; Kostenko, 1989; Kozloff, 2000b; Meyer-Wachsmuth et al., 2014; Peebles, 1915; Perea-Atienza et al., 2013; Raikova et al., 1995; Riser, 1987; Shannon and Achatz, 2007; Steinböck, 1966; Sterrer, 1998; Watzin, 1984)**.** Phylogeny of Acoelomorpha from Jondelius et al., 2011 and Albade and Jondelius, 2024.

Methods

Animal husbandry

We reared gravid *H. miamia* in communal plastic 2.25 L tanks with approximately 1.25 L of artificial seawater (37 ppt, pH 7.8-8.2). These communal tanks were kept in incubators held at 21°C. Twice weekly, we collected embryos, changed their seawater, and fed them with *Artemia* sp. (brine shrimp). The embryos were raised in petri dishes. Once they hatched, we transferred

746 juvenile worms to tanks maintained at room temperature and fed them with marine rotifers
747 (*Brachionus plicatilis*). When reproductive organs began to develop, we transferred worms to
748 larger tanks, each typically housing 30-50 worms. To pair animals for mating, we transferred
749 juvenile worms from tanks to 24-well plates and reared them in isolation following similar
750 feeding and cleaning routines as listed above. In order to study the regeneration of reproductive
751 systems, we isolated adult worms from communal tanks, anesthetized them in 15% tricaine
752 (ethyl 3-aminobenzoate methanesulfonic acid), and then amputated them with micro knives
753 (Fine Science Tools #10316-14). We maintained regenerating worm fragments in 6-well plates
754 and cleaned plates twice weekly. Five days after amputation, we fed these worms *Artemia* sp.
755 (brine shrimp) or rotifers. We also maintained starving animals in 6-well plates that we cleaned
756 twice weekly but that were not fed. All animals are derived from an inbreeding population of
757 worms collected in 2010 from Bermuda.
758
759 **Histology**
760 We fixed adult specimens of *H. miamia* in 4% paraformaldehyde in artificial seawater for 24
761 hours at room temperature. Following fixation, specimens were washed twice with 70% ethanol
762 to remove the fixative and then preserved in a third change of 70% ethanol for histological
763 preparation. Animals were dehydrated through a graded ethanol series (95% and 100%),
764 cleared in Histoclear, and embedded in Leica Surgipath (Paraplast) with a melting point of 56°C.
765 We made longitudinal, transverse, and sagittal sections at a thickness of 5 μm using a Leitz
766 1512 microtome. Histological sections were deparaffinized using Histoclear and rehydrated
767 through a graded ethanol series (100%, 95%, 70%, and 50%) to distilled water. Following
768 rehydration, sections were stained using a standard Hematoxylin and Eosin (H&E) protocol
769 (Armed Forces Institute of Pathology, 1960). Specifically, slides were incubated in Harris
770 Hematoxylin, rinsed with tap water, differentiated in acidic ethanol (70% ethanol with
771 hydrochloric acid), blued in alkaline water (distilled water with ammonium hydroxide), and

772 counterstained with Eosin. After staining, sections were dehydrated through ascending ethanol
773 concentrations, cleared in Histoclear, air-dried overnight, and mounted on glass slides with
774 Permount. Images were acquired using a Zeiss Axio Scan.Z1, and an Olympus BX50
775 microscope.
776
777 **Fluorescence *in situ* hybridization (FISH)**
778 We synthesized riboprobes following protocols established in (Srivastava et al., 2014).
779 Following 1-2 weeks of starvation, we fixed whole worms in 4% paraformaldehyde in artificial
780 sea water for one hour at room temperature. We then washed the fixed animals with PBST
781 (PBS + 0.1% Triton-X-100) and transferred them to 24-well plates in small baskets with a mesh
782 bottom, with 4-6 animals in each basket. To remove pigment autofluorescence, we treated the
783 animals with a bleach solution (containing 4% hydrogen peroxide, SSC, and formamide) and left
784 them under a light for two hours. For all washes, 800 µL of solution was used. We first
785 permeabilized the animals using proteinase K solution (0.1% SDS, 1 µL/10 mL proK in PBSTx).
786 After 10 minutes, we post-fixed the worms in 4% formaldehyde in PBST, washed twice in PBST,
787 and then washed in a 1:1 PBST:PreHyb solution for 10 minutes. We then incubated the
788 samples in PreHyb solution (50% DI formamide, 25% 20X SSC, 0.05% 10% Tween-20, 1mg/mL
789 yeast tRNA, 20% water) for two hours in a 56°C hybridization oven and then transferred them to
790 a hybridization solution (50% DI formamide, 25% 20X SSC, 0.05% 10% Tween-20, 1 mg/mL
791 yeast tRNA, 10% 50% dextran sulfate, 10% water) containing riboprobe(s) overnight. We then
792 put the specimens through several 30-minute washes at 56°C, starting with two PreHyb
793 washes, two 1:1 PreHyb:2XSSCT washes, two 2XSSCT (2XSSC with 0.1% TritonX-100)
794 solution washes, two 0.2XSSCT (0.2X SSC with 0.1% TritonX-100) solution washes. We cooled
795 the specimens to room temperature and then washed them in two ten-minute PBST washes.
796 We then performed a 1-hour blocking at room temperature with blocking solution (5% horse
797 serum and 5% casein in PBST). We incubated specimens with anti-Digoxigenin-POD (1:1500

798 dilution; Roche, 11633716001) in a blocking buffer overnight. The following day, we washed
799 animals 6 times with PBST, incubated with a tyramide buffer (1.1688g/mL NaCl, 6.18mg/mL
800 boric acid, filled with water and adjusted pH to 8.5) for 10 minutes, then developed with
801 rhodamine-conjugated tyramide solution for 10 minutes. We washed animals again with PBST
802 and incubated for 1 hour in 1:500 PBST:Hoechst to label nuclei. We mounted the animals on
803 glass slides with VECTASHIELD® PLUS Antifade Mounting Medium (Vector Laboratories, H-
804 1900). We estimated worm length (Fig. 4A-D) by measuring copulatory apparatus length
805 (gonopore to prostatic vesicle) or cross-sectional worm width within the image and comparing
806 that measurement to measurements of developing worms.
807
808 **Whole-mount immunofluorescence**
809 We fixed worms in 4% paraformaldehyde (Electron Microscopy Sciences, 15714) in artificial sea
810 water for 1-2 hours at room temperature (juveniles were fixed for one hour, adults were fixed for
811 two) before washing with PBST (PBS + 0.1% Triton-X-100). We anesthetized adult worms in 0.5
812 mg/mL tricaine for 5 minutes prior to fixation to minimize epidermal rupture. For
813 immunofluorescence, we washed worms in PBST, blocked for one hour at room temperature in
814 10% goat serum in PBST, and incubated them in primary antibody for 48-72 hours at 4°C on a
815 shaker (juveniles for 48 hours, adults for 72 hours). The following day, we washed worms
816 thoroughly in PBST (8 x 20 min washes) on a nutator before blocking for one hour at room
817 temperature on a shaker. We incubated worms in secondary antibody overnight at 4°C; the
818 following day, we washed them thoroughly in PBST (8 x 20 in washes) on a shaker before
819 adding direct conjugate dyes and mounting them on glass slides with VECTASHIELD®
820 HardSet™ Antifade Mounting Medium (Vector Laboratories, H-1400-10). We used the following
821 antibodies: Tropomyosin (custom) (Hulett et al., 2020), Piwi-1 (custom), Goat anti-Rabbit IgG
822 (H+L) Cross-Adsorbed Secondary Antibody, Alexa Fluor™ 568 (ThermoFisher, A-11011),
823 Hoechst (ThermoFisher, H1399), SiR-actin (Cytoskeleton, CY-SC001) and FMRFamide

824 (EMDMillipore AB15348). These antibodies were selected because, in previous work, we found
825 that they labeled relevant morphological structures in *Hofstenia*. We acquired all images with
826 FISH and immunofluorescence on a Leica SP8 point-scanning confocal microscope. We
827 generated the Piwi-1 (Rabbit polyclonal) custom antibody using GenScript as previously
828 described for Tropomyosin (Hulett et al., 2020). Briefly, a peptide was synthesized from the *H.*
829 *miamia* Piwi-1 protein sequence, expressed in *E. coli,* and used to immunize rabbits. The Piwi-1
830 antibody used in this paper was #SC1195 (0.845 mg/mL), used at the concentration of 2 ug/mL.
831
832
833 **Quantitative analysis of development, regeneration, and de-growth**
834 We collected 42 zygotes laid from wild-type worms. Two embryos did not hatch, and two worms
835 died during the course of the experiment (likely due to handling error). Four worms were
836 removed from the experiment at different timepoints for additional imaging, resulting in 34
837 worms that we followed into adulthood (Fig. S2B). We transferred each embryo to a well of a
838 24-well cell culture plate with artificial seawater. Plates were stored in a temperature-controlled
839 incubator. Without removing the embryos from the plate, we imaged them twice weekly through
840 a dissection microscope with white illumination from LEDs mounted above the sample. We also
841 changed water on these days. We added the same volume of water to each well (2.35 mL in
842 each 12-well). Once at least one embryo had hatched, we added rotifers to each well. On each
843 feeding day, we calculated the concentration of rotifers by counting the number of rotifers in
844 diluted samples. Based on this concentration, we changed the volume of rotifers added to each
845 well to ensure a consistent number of rotifers was given to each animal. At different stages
846 during the experiment, we increased the number of rotifers (Fig. S2A). These increases were
847 gradual to ensure worms always had more food than they could eat, while minimizing excess
848 food which could affect water quality. We removed hatched worms from wells for imaging twice
849 weekly. We anesthetized worms in tricaine, and mounted them on microscope slides with a

850 20x20 mm sticker grid with 1mm resolution (ThomasScientific, #1207X53). Depending on the
851 worms' pigmentation, this grid is visible through the body of some worms, but this did not impact
852 the visibility of reproductive organs. When worms were larger, we moved them to larger 6-well
853 plates in 10 mL of artificial sea water and began to feed them brine shrimp in addition to rotifers
854 (Fig. S2A). We measured the number of brine shrimp added using the same concentration
855 procedure outlined above for rotifers. Once worms had matured, we increased the number of
856 brine shrimp.

857 We manually annotated images in FIJI. We measured lengths from the most posterior
858 part of the male reproductive system (e.g., base of the penis tube before sperm production
859 begins or base of the seminal vesicle) to the male gonopore, the length of the seminal vesicle,
860 the length of each ovary, the length of the worm's body, and the width of the worm's body. We
861 calculated penis length by subtracting the length of the seminal vesicle from the length of the
862 male gonad. All measurements were converted to millimeters using image-specific scale
863 information.

864 We repeated these imaging and measurement processing procedures with starving
865 worms and regenerating worm fragments. We anesthetized and imaged starved and fed control
866 worms roughly once a week for 11 weeks. 106 days after isolation, we imaged the starved
867 worms again, at which point one starved worm had died. We imaged regenerating worms
868 starting 2 days post-amputation and then again every 2-5 days until 25 days post-amputation at
869 which point we took images less frequently. We did not feed regenerating fragments for the first
870 four days after amputation, and then fed them normally. In these experiments, we used a two-
871 pointed line or multi-jointed line to measure lengths. We performed all analyses in python, with
872 code assistance from GPT4.

873

874 **Egg-laying behavior**

875 We moved adult worms from a communal tank to individual wells in the center of a 24-well plate
876 or 12-well plate (Fisher Scientific #07-200-82). We mounted the plate on an elevated platform
877 within an enclosed behavioral rig. The plate was illuminated with uniform white light, from
878 addressable LEDs (Adafruit #SK6812RGBW, powered by 5V DC) arranged in a ring around the
879 plate behind a white acrylic diffuser (McMaster-Carr #8505K741). An infrared camera (Basler
880 Ace ac4024-29um USB 3.0 monochrome) was mounted underneath the plate to allow filming of
881 the worm's ventral surface. A USB fan was mounted on the floor of the behavioral chamber for
882 temperature regulation. We filmed worms at 1Hz for 8-12 hours. After filming, each worm was
883 returned to its original communal tank.

884 To determine the timing of egg laying in adults with continuous access to mates, we
885 collected adult worms from communal tanks and each was placed in an individual well of a 6-
886 well plate. Every 3-4 days, we counted the number of eggs laid by each worm, removed the
887 eggs, changed the water, and fed worms with brine shrimp or rotifers. To induce self-
888 fertilization, we moved juvenile worms with immature reproductive systems from communal
889 tanks to 24-well plates and fed them with rotifers. Once these worms had increased in size, we
890 moved them to 6-well plates and fed with artemia. We recorded egg counts every 3-4 days
891 when water and food were refreshed. To determine the time course of egg laying after mating
892 once, we isolated juvenile worms. Once these worms were reproductively mature, we paired
893 each worm with another isolated worm and allowed them to mate. After mating, we returned the
894 worms to isolation. We recorded egg counts as previously described. If worms stopped laying
895 eggs for more than two weeks, we allowed them to mate again before re-isolating them.

896 To find egg positions, we maintained communal tanks according to our husbandry
897 protocol. Every 3-4 days, before cleaning, we recorded images of each face of the tank (2 short
898 faces, 2 long faces, and the floor of the tank). We then scored the x- and y-coordinates of eggs
899 on each face using FIJI. Since few eggs were laid on the floors of the tanks and it was unclear
900 whether these eggs were attached or had been dislodged from the walls of the tanks, we did not

901 score their locations (Fig. 6F). We also scored the x- and y-coordinates of the boundaries of the
902 water in each image. From these image-specific boundaries, we calculated a common set of
903 bounds for each type of face (i.e., short, long). We scaled egg coordinate positions and aligned
904 them to common bounds for analysis of spatial egg laying preferences. To ask whether worms
905 add to existing clutches of eggs, we cared for communal tanks as previously described but did
906 not remove eggs from their faces. We took images of each face, and then we transferred each
907 cohort of worms in a tank to a different tank. After 3-4 days, we took images of tank faces again,
908 scored coordinates of each egg, and recorded whether each egg was old or newly laid.
909 For experiments measuring how worms altered their egg-laying behavior based on food
910 availability, we selected 17 and 18 communal worm tanks respectively. On the first day of the
911 experiment, half of these tanks were randomly selected to have food (brine shrimp) withheld.
912 After four days with or without food, we collected and counted eggs from all tanks. To test
913 whether egg laying recovers when unfed worms are fed, we randomly selected communal tanks
914 of adult worms to have food withheld. Four days after food was added or withheld, we removed
915 all eggs that were laid, and then fed all communal tanks. Three days later, eggs were collected
916 and counted.
917
918
919 **Author Contributions**
920 VC, SET, and MS designed the project; SET and VC performed development, physiology and
921 behavior experiments; VC and SET analyzed the data; APK performed and interpreted
922 immunofluorescence and imaging experiments; DMB performed and interpreted histology
923 experiments; VC, SET, and MS wrote the manuscript with input from all authors; and MS
924 supervised the project.
925
926 **Acknowledgements**

We thank Gonzalo Giribet, Matthew Hooge, James Hanken, Javier Ortega-Hernandez, Andrew Berry, and all members of the Srivastava lab for helpful discussion. We also thank James Hanken, Júlia Chaumel, and Christina Daly for histology help and infrastructure. VC and APK are Fellows of the Jane Coffin Childs Fund for Medical Research. ST acknowledges funding from the Harvard Museum of Comparative Zoology, Herchel Smith Undergraduate Science Research Program, and the Program for Research in Science and Engineering. This project was supported by grants from the National Institute of General Medical Sciences of the NIH to MS: R35GM128817 and R35GM153252.

Data Availability

All data and code for quantitative analyses in this manuscript are available at Zenodo, DOI: https://zenodo.org/records/16923213.

Supplement

Table S1: Survey of reproductive traits within Acoelomorpha. see attached .xlsx file

Table S2: Body length is a better predictor of organ length than age in multiple regression. Multiple regression coefficients and associated p-values are reported for each organ. Wald's test was used on coefficients to test whether they are significantly different from each other.

organ	day coefficient	day p-value	worm length coefficient	worm length p-value	wald's test p-value
penis	0.0684	0.0002	0.1639	<0.0005	0.0082
seminal vesicle	0.0425	0.0003	0.0985	<0.0005	0.0128
ovary	0.3361	<0.0005	1.0029	<0.0005	<0.0005

Table S3: ANCOVA of the relationship between organ size and body size.

	F-statistic	p-value	η^2
penis	15.820	<0.0005	0.040
seminal vesicle	24.329	<0.0005	0.069
ovary	58.905	<0.0005	0.175

Table S4: Glossary of anatomical and reproductive traits.

mouth: approximate position of the mouth on the ventral surface	
central	mouth located between the anterior end and midpoint of the ventral surface
anterior	mouth located between the anterior end and midpoint of the ventral surface
posterior	mouth located between the midpoint of the ventral surface and posterior end
none	no mouth
gonad(s): tissue or organ where gametes are specified	
mixed	sperm and eggs are produced within the same tissue or organ
separate	sperm and eggs are produced in distinct tissues or organs
penis: male copulatory organ	
needle-like	penis contains hardened, sclerotized elements
muscular	absence of hardened elements; soft or glandular penis
none	penis is absent
testes: tissue where sperm are produced	
paired	there are two distinct regions where sperm are produced

unpaired	there is a single region where sperm are produced
ovaries: tissue where oocytes are produced	
paired	there is are two distinct regions where oocytes are produced
unpaired	there is a single region where oocytes are produced
fem. gonopore: female genital opening	
present	a female genital opening is present
absent	a female genital opening is not present
bursa: an organ used to hold sperm received during mating	
present	a bursa is present
absent	a bursa is not present
# bursal nozzles: the number of channels accompanying the bursa; channels that facilitate sperm movement or modification	
0	the bursa is not accompanied by any sperm channels
1	the bursa has one channel used to move sperm
>1	the bursa has more than one channel used to move sperm
egg laying: the mode of oviposition that a species has been observed to use	
mouth	eggs are deposited via the mouth
fem. gonopore	eggs are deposited via the female genital opening

body wall rupture	eggs are deposited via breaks in the body wall
mating: the mode of sexual reproduction that a species has been observed to use	
hypodermic	a copulation mode where sperm is injected beneath the epidermis of a partner
hyperdermal	a copulation mode where sperm are deposited on the epidermis of a partner
true copulation	penis inserted in the female gonopore of a partner; insertion can be mutual or one-sided
alt. reproductive strategies: forms of reproduction other than two individuals mating	
fission	splitting of an individual into two or more individuals
budding	development of an outgrowth and then detachment of that outgrowth to form offspring
self-fertilization	zygote forms from fusion of sperm and egg from a single individual

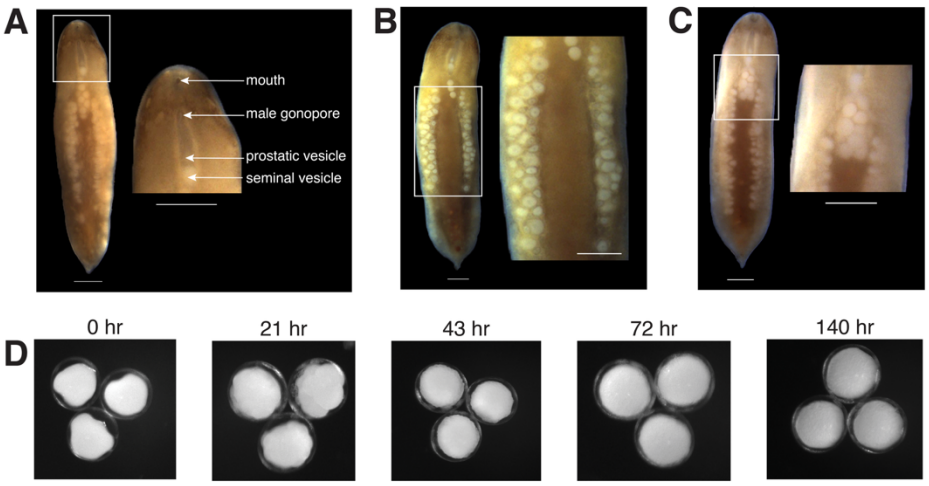

Figure S1: Gross reproductive morphology of *H. miamia* seen in a ventral view. (A) The male reproductive system includes the male gonopore, penis, prostatic vesicle, and seminal vesicle. (**B**) *H. miamia*'s ovaries are lateral, and organized along the anterior-posterior axis. There is no visible

organization of oocytes by size or stage within the ovaries. (**C**) A cluster of zygotes is visible medially, and immediately posterior to the male copulatory apparatus. (**D**) Representative time course of embryonic development of embryos dissected from the central cavity. Scale bars: 1 mm.

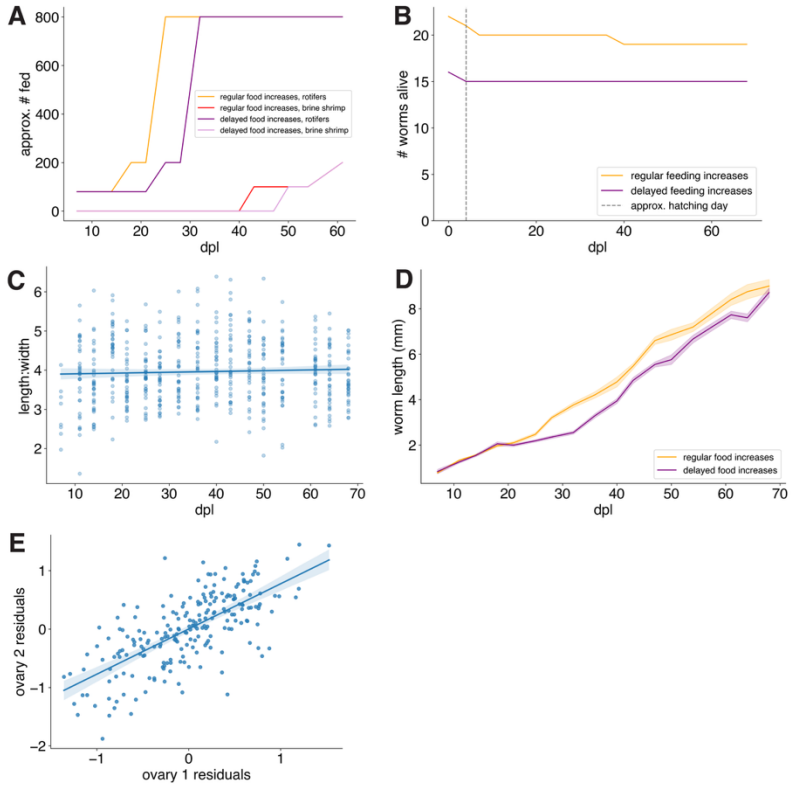

Figure S2: Growth and scaling patterns in juvenile development. (**A**) Time course of feeding changes through juvenile development, showing the delayed increases in feeding for one group, and the introduction of brine shrimp late in development. (**B**) Survival curve showing the number of worms in each of the two feeding treatments over time. (**C**) The aspect ratio (length:width) of worms is consistent over time (slope = 0.002, R^2 = 0.002, p = 0.31), showing that worms grow proportionally over development. Error band shows 95% confidence interval. (**D)** Worm length increases over time, with worms growing more slowly when their increased feeding was delayed. Error band shows SEM. (**E**) Residuals of ovary length (regressed against body length) within each worm are highly correlated (Pearson correlation coefficient = 0.7, $p < 0.0001$). Error band shows 95% confidence interval.

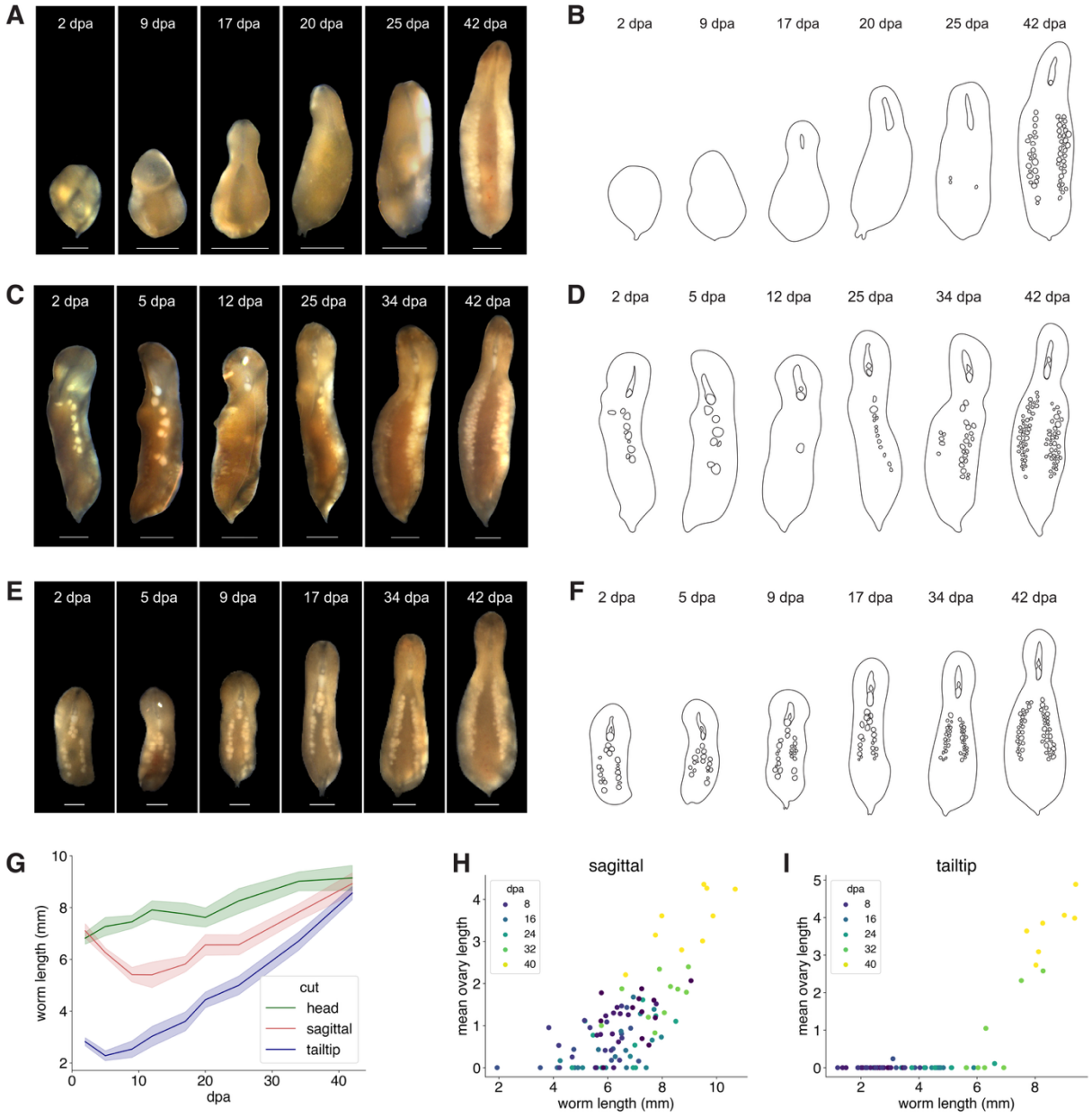

Figure S3: Reproductive system regeneration dynamics from different initial configurations. (**A, C, E**) Representative time course of regenerating tail tip, sagittal cut, and head, and (**B, D, F**) schematized version with reproductive structures shown. (**G**) Regenerating heads and tail tips increase in length following amputation while sagittally-cut fragments shrink and then begin to grow. Error bar shows SEM. (**H**) Ovaries scale with body length in sagittally-cut fragments. (**I**) Ovaries regenerate once a tail fragment reaches a certain length. Scale bars: 1 mm.

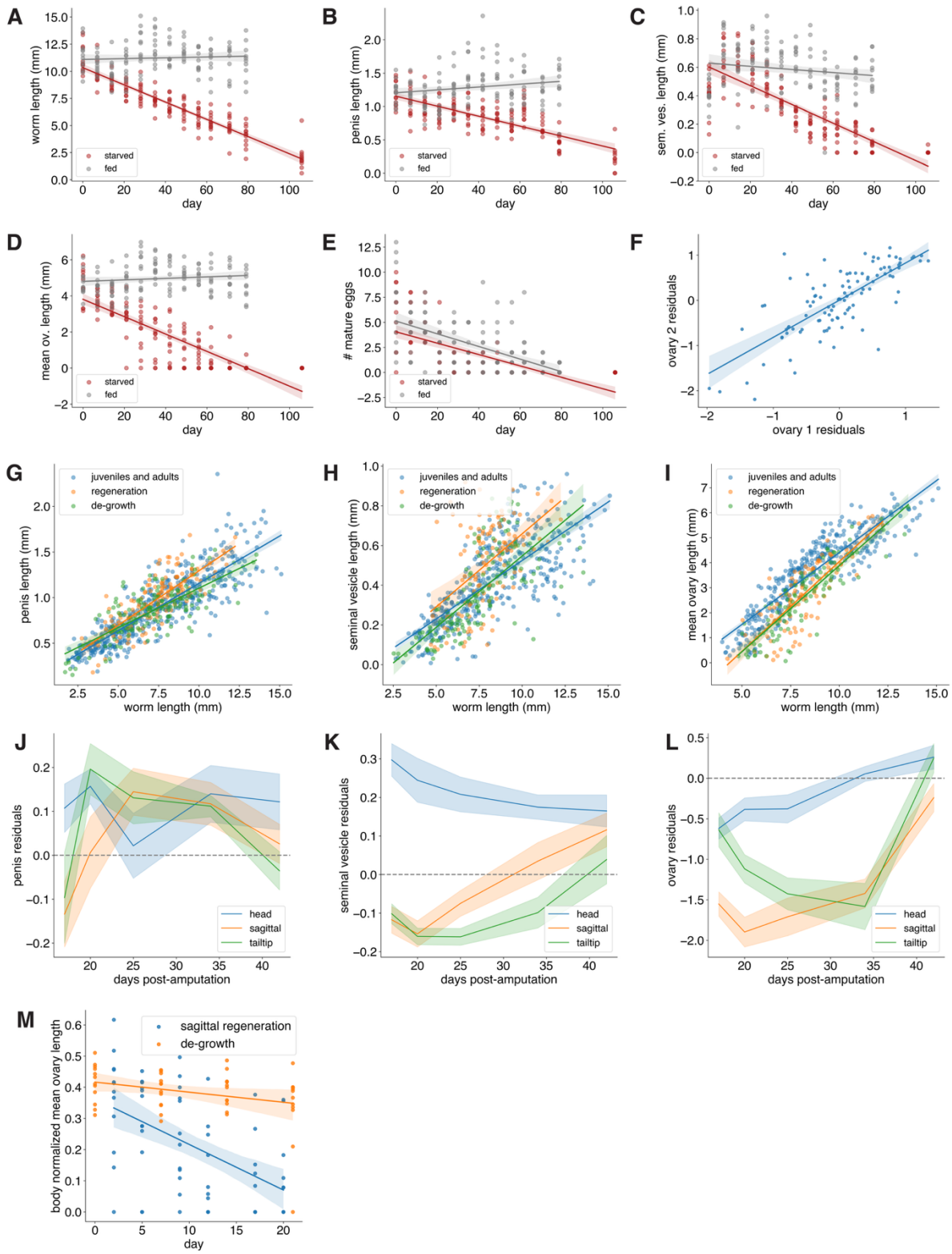

980

981 **Figure S4: Across different growth contexts, body and organ scaling rules are conserved.** (**A**)

982 Worm length decreases over time when worms are starved (starved: $R^2 = 0.85$, $p < 0.0001$; fed control:

983 $R^2 = 0.004$, $p = 0.48$). Error band shows 95% confidence interval. (**B-D**) Penis length (starved: $R^2 = 0.54$,
984 $p < 0.0001$; fed control: $R^2 = 0.04$, $p = 0.03$), seminal vesicle length (starved: $R^2 = 0.60$, $p < 0.0001$; fed
985 control: $R^2 = 0.03$, $p = 0.06$), and mean ovary length (starved: $R^2 = 0.67$, $p < 0.0001$; fed control: $R^2 =$
986 0.02, $p = 0.15$) decrease over time for worms experiencing de-growth but do not change in worms that
987 are continuously fed. Error band shows 95% confidence interval. (**E**) The number of zygotes in the central
988 cavity decreases over time in both starved and fed worms, likely because these worms are isolated
989 (starved: $R^2 = 0.48$, $p < 0.0001$; fed control: $R^2 = 0.33$, $p < 0.0001$). Error band shows 95% confidence
990 interval. (**F**) When controlling for the effect of body size, the residuals of ovary length (regressed against
991 body length) are strongly correlated between ovaries within worms over the course of de-growth (Pearson
992 correlation coefficient = 0.75, $p < 0.0001$). Error band shows 95% confidence interval. (**G-I**) The size of
993 reproductive structures scale similarly (see Table S3) across development, de-growth, and regeneration
994 (penis $R^2 = 0.70$, $p < 0.0001$; seminal vesicle: $R^2 = 0.50$, $p < 0.0001$; ovary: $R^2 = 0.76$, $p < 0.0001$). Error
995 band shows 95% confidence interval. All data here are from regenerating fragments at least two weeks
996 post-amputation, when worms begin regenerating their reproductive organs. **(J-L**) The residuals of organ
997 length (regressed against body length) generally converge towards zero over the course of regeneration
998 despite sometimes displaying large initial deviations. Data from regenerating fragments prior to two
999 weeks omitted. (**M**) Sagittal fragments degrade their existing ovary during initial regeneration at a faster
1000 rate normalized to body size (slope = -0.015) than adult worms experiencing de-growth (slope = -0.003)
1001 (Wald's test on slope of linear regression of ovary length and day: p=0.0006). Error band shows 95%
1002 confidence interval.
1003

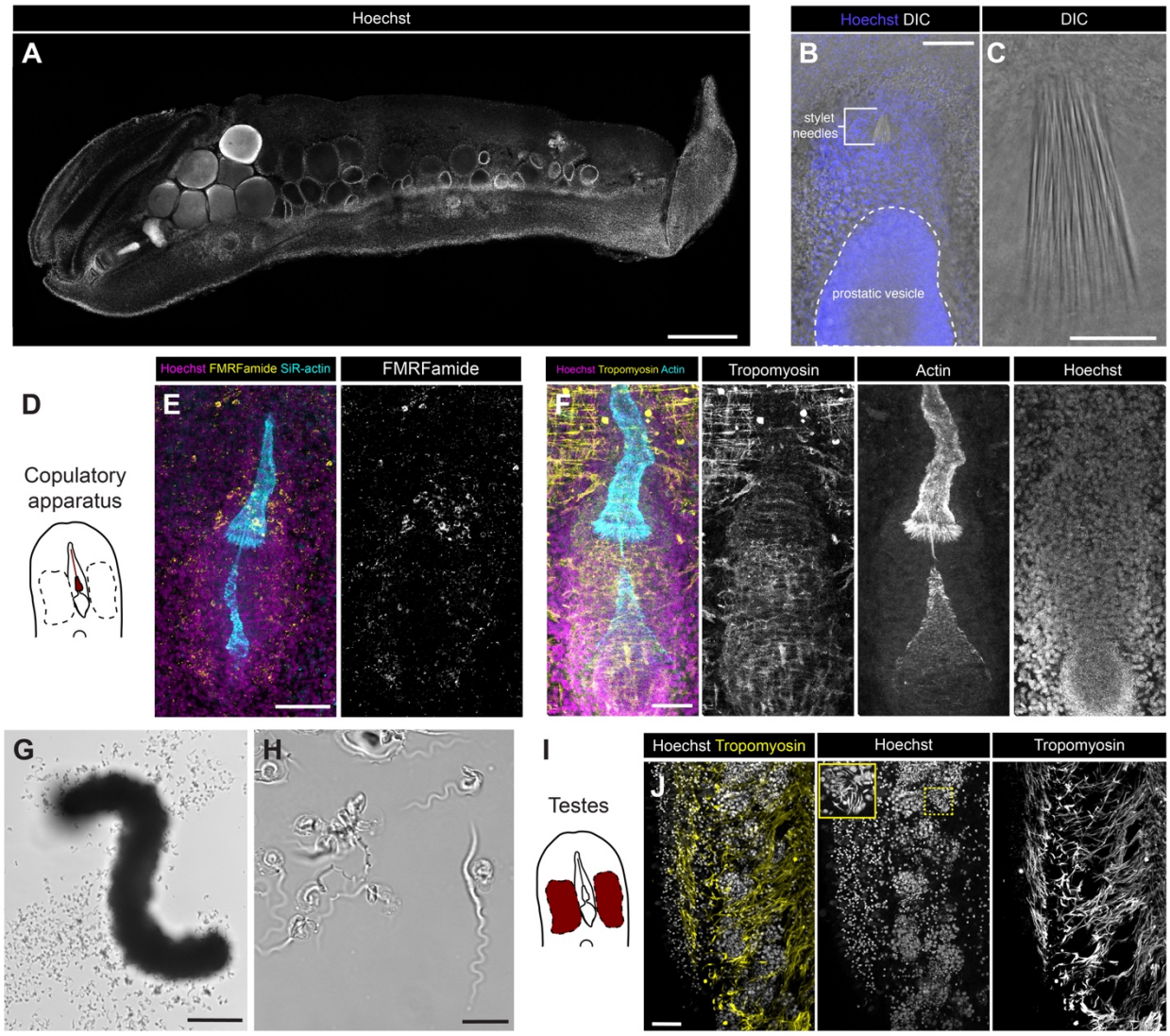

1004

1005 **Figure S5: Fine structure of *H. miamia*'s male reproductive system.** (**A**) The gross morphology and
1006 location of the reproductive system can be seen in sagittally-cut worms with nuclear staining. (**B-C**) Penis
1007 stylets are arranged in a bundle, seen with differential interference contrast (DIC). (**D**) Schematic of the
1008 male reproductive structures with the copulatory apparatus highlighted. (**E**) Antibody staining for
1009 FMRFamide shows that the penis sheath is surrounded by presumptive neurons. (**F**)
1010 Immunofluorescence for tropomyosin, and actin and nuclear labeling enables visualization of the
1011 musculature surrounding the male structures. (**G**) A packet of sperm ejected during mating made up of
1012 (**H**) sperm cells. (**I**) Schematic of the male reproductive structures with the testes highlighted. (**J**) Sperm in
1013 the testes develop in clusters interspersed with the muscle of the body, visualized by

1014 immunofluorescence for Tropomyosin, a muscle marker. Scale bars: 500μm (A), 100μm (B, G), 50μm (C,

1015 E, J), 25μm (F), 10μm (H).

1016

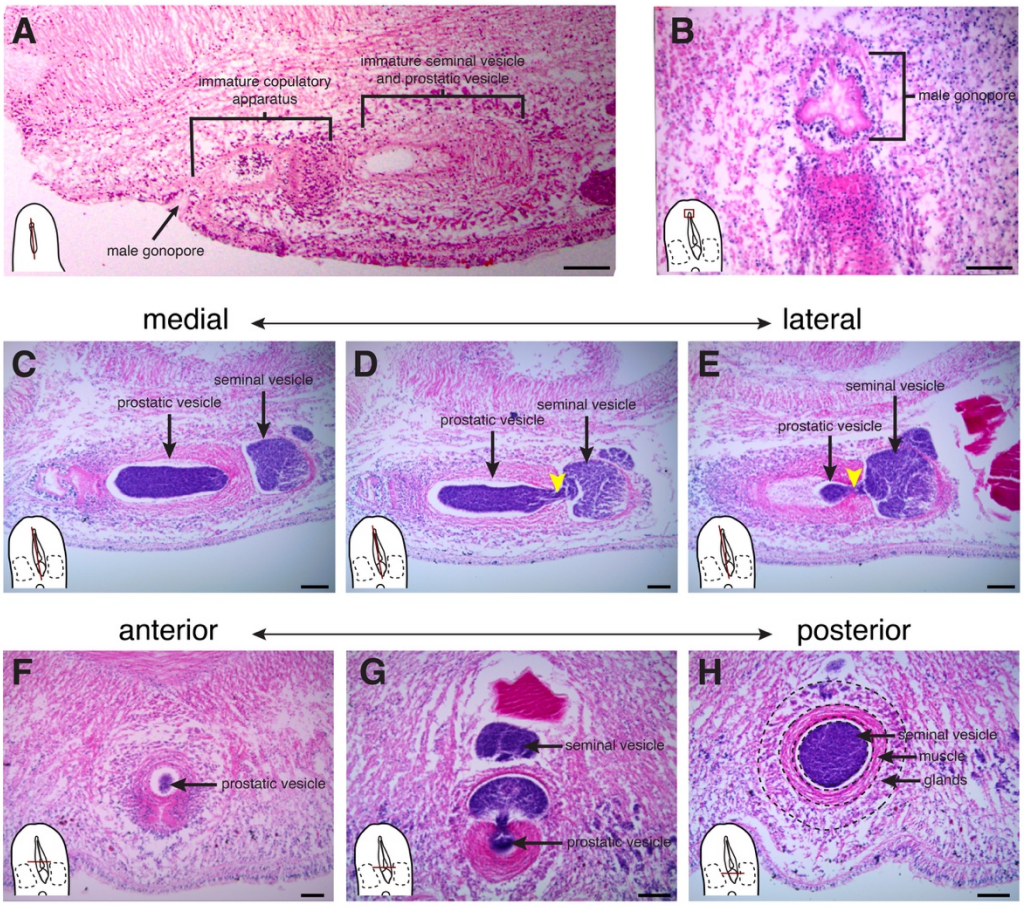

1017

1018 **Figure S6: Histology of the male reproductive system. (A)** The male reproductive system in a sagittal

1019 section of a juvenile worm has a male gonopore but lacks a clear male copulatory apparatus, prostatic

1020 vesicle, and seminal vesicle. **(B)** A longitudinal section showing the male gonopore. **(C-E)** Sagittal

1021 sections through the male reproductive system along the medial-lateral axis showing a channel of sperm

1022 (yellow arrows) connecting the prostatic vesicle and seminal vesicle. **(F-H)** Transverse sections moving

1023 along the anterior-posterior axis show the positions of the prostatic vesicle and seminal vesicle and the

1024 musculature and glands surrounding the seminal vesicle. Scale bars: 100 um.

1025

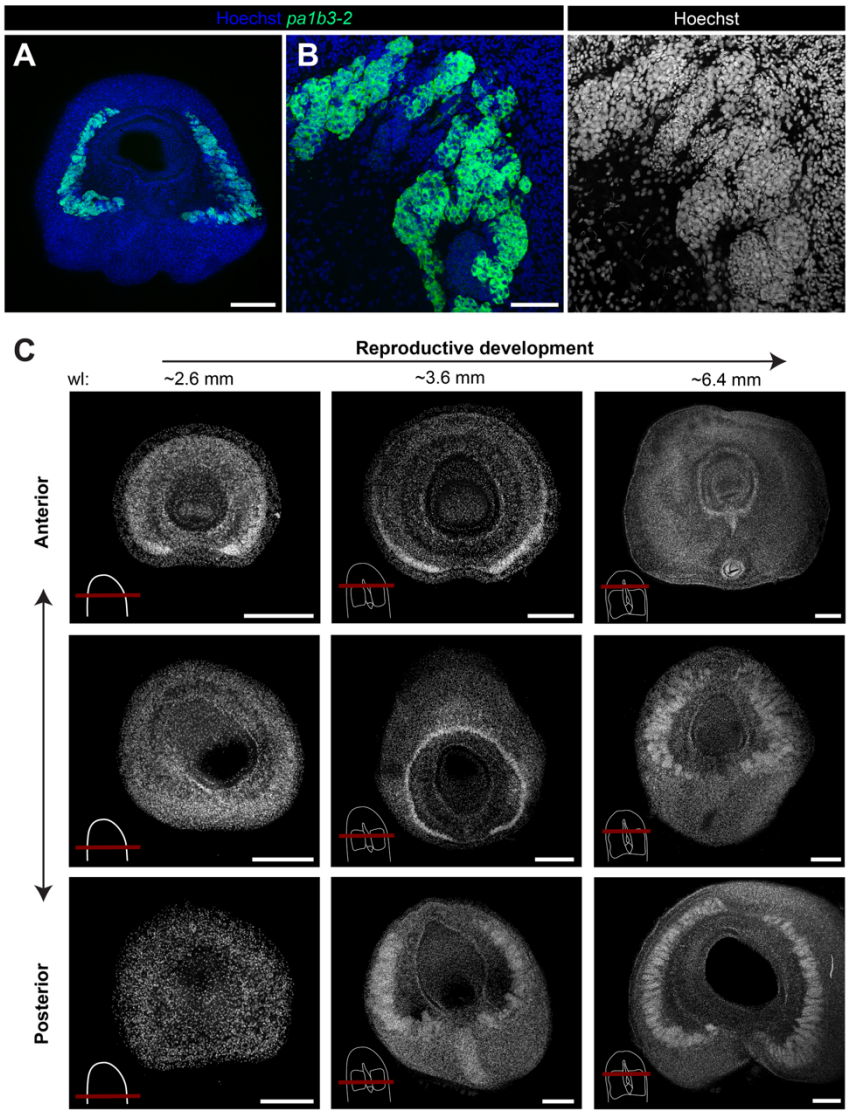

1026

1027 **Fig. S7: Testes emerge as lateralized regions and grow to span the dorsal surface as**

1028 **worms grow.** (**A**) FISH for the male germline marker *pa1b3-2* results in two regions of

1029 ventrolateral expression that extend toward the dorsal surfaces. (**B**) Hoechst and *pa1b3-2*

1030 mRNA expression label sperm cells. (**C**) Nuclear staining of cross-sections at different points

1031 along the anterior-posterior axis within the head shows that the testes emerge as two lateral

1032 lobes that gradually form a continuous cylindrical structure. Cartoons depict the plane of

1033 sectioning (red line) and reproductive structures (white). Scale bars: 250 µm (A), 50µm (B),

1034 200µm (C).

1035

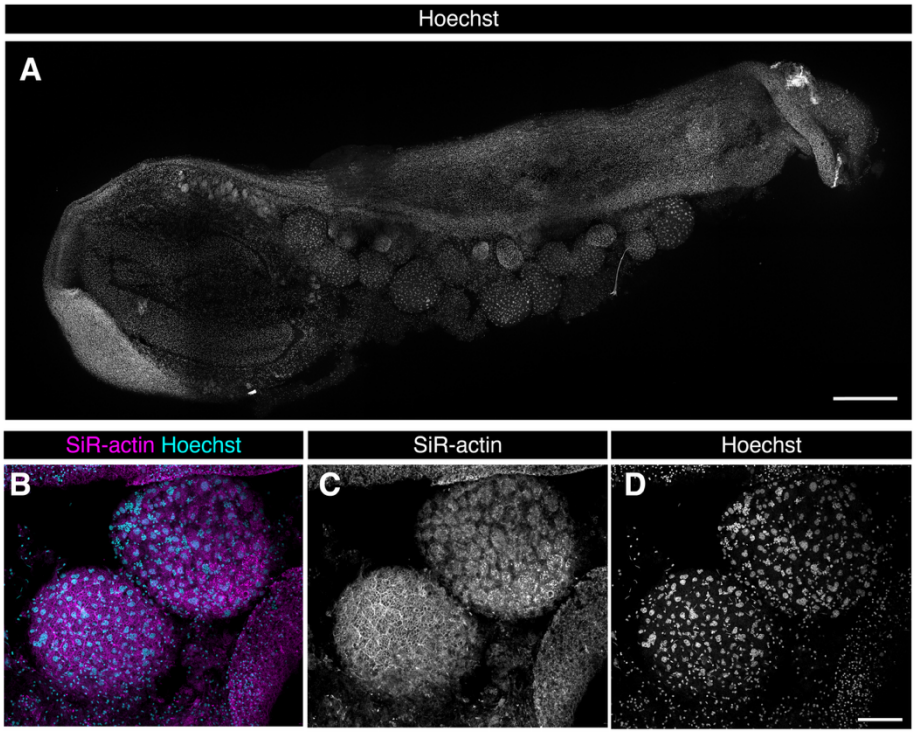

1036

1037 **Figure S8: Oocytes in *Hofstenia*'s ovaries are surrounded by follicular cells.** (**A**) Nuclear staining on
1038 a sagittally-cut worm confirms the presence of ovaries along the ventral side of the worm. Consistent with
1039 our other imaging, ovaries lack any sense of organization in regards to maturity along the anterior-
1040 posterior axis. (**B-D**) Oocytes are surrounded by a layer of follicular cells. Scale bars: 500μm (A), 100μm
1041 (D).

1042

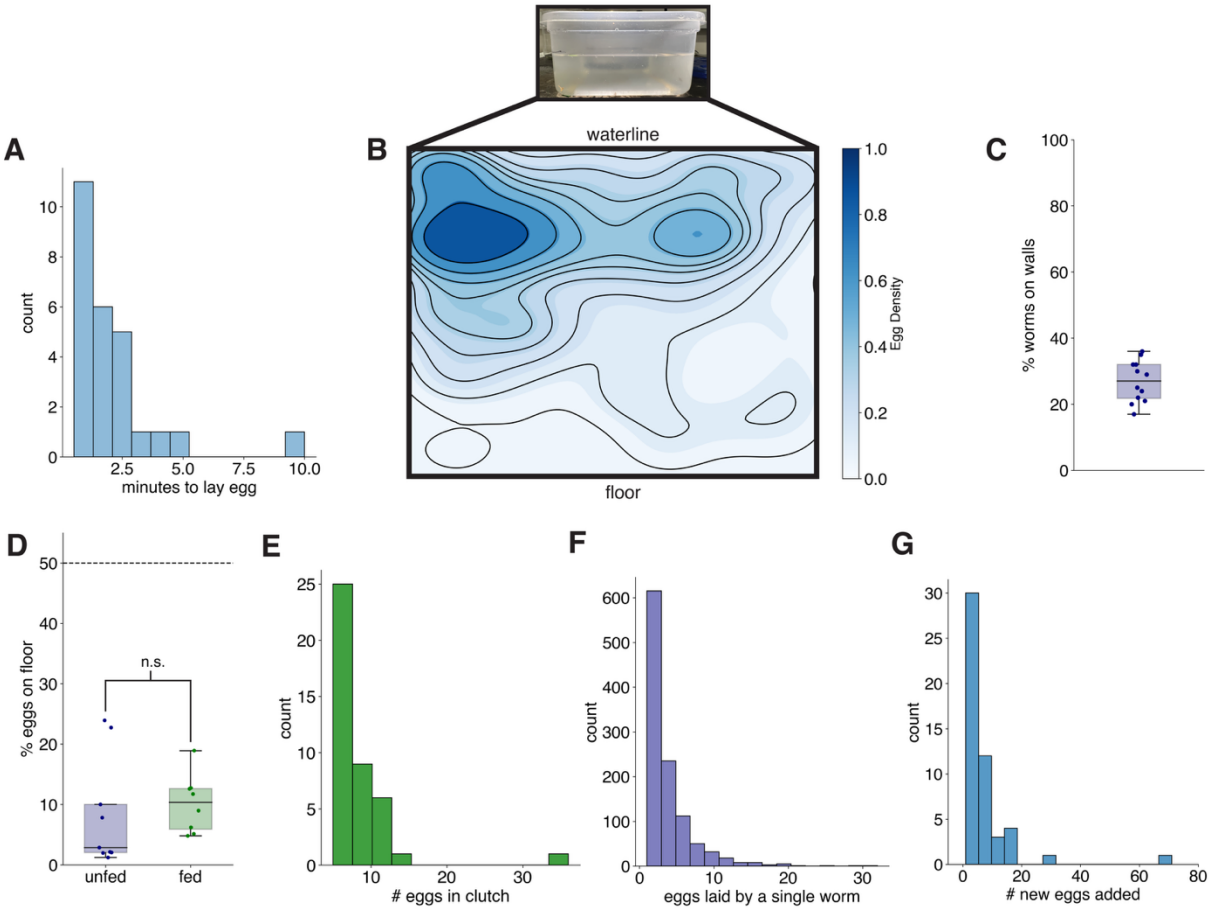

Figure S9: Worms have spatial preferences during egg-laying. (**A**) Quantifying the time from the start of visible muscle contractions to egg laying reveals that the egg-laying process spans a timescale of seconds to minutes for each egg, with most eggs being laid within 3 minutes. (**B**) Kernel density estimate of egg locations on the short walls of the worm tanks (n = 1390 eggs). (**C**) Random observations of worms in their culture tanks (n = 12 tanks) finds only a minority of worms on the upper half of tank walls, even in conditions where we expect them to be actively laying eggs. (**D**) Worms preferentially avoid laying eggs on the floor of the tank regardless of whether they are fed or unfed (two-sample t-test: p= 0.62, n ≥ 8). (**E**) Distribution of clutch sizes in communal tanks (n = 42 clutches) shows that clutches frequently contain more than 10 eggs laid within a 3-4 day window. (**F**) Distribution of eggs laid by individual worms across different egg laying contexts shows that most worms lay fewer than 10 eggs in a 3-4 day window

(**G**) Worms often add eggs to clutches constructed by other worms; the distribution shows the numbers of new eggs added to old clutches.

Video 1: The penis sheath is ciliated. Live-imaging of the ventral surface of a worm shows beating cilia lining the sheath. This set of cilia is distinct from the cilia lining the epidermis of the worm.

Video 2: The male gonopore is ciliated. Live imaging of the ventral surface of a worm shows that the male gonopore has beating cilia.

Video 3: Eggs are laid through the mouth. Video of an adult worm laying eggs, filmed from the ventral surface at 1Hz and sped up 2000x. The worm lowers its mouth and then contracts its body. During these contractions, a cluster of mature eggs can be seen distending the body. An individual egg is loaded into and travels through the pharynx eventually emerging through the mouth.

References

Abalde S, Jondelius U. 2024. A phylogenomic backbone for Acoelomorpha inferred from transcriptomic data. *Syst Biol*. doi:10.1093/sysbio/syae057

Achatz JG, Chiodin M, Salvenmoser W, Tyler S, Martinez P. 2013. The Acoela: on their kind and kinships, especially with nemertodermatids and xenoturbellids (Bilateria incertae sedis). *Org Divers Evol* **13**:267–286.

Achatz JG, Hooge MD. 2006. Convolutidae (Acoela) from Tanzania. *Zootaxa* **1362**:1.

Ahyong S, Boyko CB, Bernot J, Brandão SN, Daly M, De Grave S, de Voogd NJ, Gofas S, Hernandez F, Hughes L, Neubauer TA, Paulay G, van der Meij S, Boydens B, Decock W, Dekeyzer S, Goharimanesh M, Vandepitte L, Vanhoorne B, Adlard R, Agatha S, Ahn KJ, Alonso MV, Alvarez B, Amler MRW, Amorim V, Anderberg A, Andrés-Sánchez S, Ang Y, Antić D, Antonietto LS, Arango C, Artois T, Atkinson S, Auffenberg K, Bailly N, Baldwin BG, Bank R, Barber A, Barrett RL, Bartsch I, Bellan-Santini D, Bergh N, Bernard C, Berrios Ortega FJ, Berta A, Bezerra TN, Bieler R, Blanco S, Blasco-Costa I, Blazewicz M, Błędzki LA, Bock P, Bonifacino M, Böttger-Schnack R, Bouchet P, Boury-Esnault N, Bouzan R, Boxshall G, Bray R, Brito Seixas AL, Bruce NL, Bruneau A, Budaeva N, Bueno-Villegas J, Calvo Casas J, Cárdenas P, Carstens E, Cartwright P, Cedhagen T, Chan BK, Chan TY, Chernyshev A, Choong H, Christenhusz M, Churchill M, Collins AG, Collins GE, Collins K, Consorti L, Copilaș-Ciocianu D, Corbari L, Cordeiro R, Costa VM d. M, Costa Corgosinho PH, Coste M, Costello MJ, Crandall KA, Cremonte F, Cribb T, Cuscó-Borràs J, Cutmore S, Dahdouh-Guebas F, Daneliya M, Dauvin JC, Davie P, De Broyer C, de Lima Ferreira P, de Mazancourt V, de Moura Oliveira L, Decker P, Defaye D, Dekker H, Di Capua I, Dippenaar S, Dohrmann M, Dolan J, Domning D, Downey R, Dreyer N, Eisendle U, Eitel M, Eleaume M, Enghoff H, Epler J, Esquete Garrote P, Evenhuis NL, Ewers-Saucedo C, Faber M, Figueroa D, Fišer C, Fordyce E, Foster W, Fransen C, Freire S, Fujimoto S, Furuya H, Galán-Díaz J, Galbany-Casals M, Gale A, Galea H, Gao T, García-Moro P, Garic R, Garnett S, Gaviria-Melo S, Gerken S, Gibson D, Gibson R, Gil J, Gittenberger A, Glasby C, Glenner H, Glover A, Gómez I, Gómez-Noguera SE, Gondim AI, Gonzalez BC, González-Solís D, Goodwin C, Gostel M, Grabowski M, Gravili C, Grossi M, Guerra-García JM, Guerrero JM, Guidetti R, Guiry, Gutierrez D, Hadfield KA, Hajdu E, Halanych K, Hallermann J, Hayward BW, Hegna TA, Heiden G, Hendrycks E, Hennen D, Herbert D, Herrera Bachiller A, Hodda M, Høeg J, Hoeksema B, Holovachov O, Hooge, Hooper JN, Horton T, Houart R, Huys R, Hyžný M, Iniesta LFM, Iseto T, Iwataki M, Janssen R, Jaume D, Jazdzewski K, Jersabek CD, Jiménez-Mejías P, Jóźwiak P, Kabat A, Kajihara H, Kakui K, Kantor Y, Karanovic I, Karapunar B, Karthick B, Kathirithamby J, Katinas L, Kilian N, Kim YH, King R, Kirk PM, Klautau M, Kociolek JP, Köhler F, Konowalik K, Kotov A, Kovács Z, Kremenetskaia A, Kristensen RM, Kroh A, Kulikovskiy M, Kullander S, Kupriyanova E, Lamaro A, Lambert G, Larridon I, Lazarus D, Le Coze F, Le Roux M, LeCroy S, Leduc D, Lefkowitz EJ, Lemaitre R, Lichter-Marck IH, Lim SC, Lindsay D, Liu Y, Loeuille B, Lois R, Lörz AN, Ludwig T, Lundholm N, Macpherson E, Maguilla E, Mah C, Mamos T, Manconi R, Mapstone G, Marek PE, Markello K, Márquez-Corro JI, Marshall B, Marshall DJ, Martin P, Martín-Bravo S, Martinez Arbizu P, Maslakova S, McFadden C, McInnes SJ, McKenzie R, Means J, Mees J, Mejía-Madrid HH, Meland K, Merrin KL, Míguez M, Miller J, Mills C, Moestrup Ø, Mokievsky V, Molodtsova T, Monniot F, Mooi R, Morales-Alonso A, Morandini AC, Moreira da Rocha R, Morrow C, Mortelmans J, Müller A, Muñoz Gallego AR, Muñoz Schüler P, Musco L, Nascimento JB, Nesom G, Neto Silva M d. S, Neubert E, Neuhaus B, Ng P, Nguyen AD, Nielsen C, Nielsen S, Nishikawa T, Norenburg J, O'Hara T, Opresko D, Osawa M, Osigus HJ, Ota Y, Páll-Gergely B, Panero JL, Patterson D, Pedram M, Pelser P, Peña Santiago R, Perbiche-Neves G, Pereira J d. S, Pereira PHM, Pereira SGG, Perez-

Losada M, Petrescu I, Pfingstl T, Piasecki W, Pica D, Picton B, Pignatti J, Pilger JF, Pinheiro U, Pisera AB, Poatskievick Pierezan B, Polhemus D, Poore GC, Potapova M, Praxedes RA, Půža V, Read G, Reich M, Reimer JD, Reip H, Resende Bueno V, Reuscher M, Reynolds JW, Richling I, Rimet F, Ríos P, Rius M, Rodríguez E, Rogers DC, Roque N, Rosenberg G, Rützler K, Sa IR d. S, Sá HAB, Saavedra M, Sabater LM, Sabbe K, Sabroux R, Saiz-Salinas J, Sala S, Samimi-Namin K, Sánchez-Villegas M, Sánchez-Villegas R, Santagata S, Santos S, Santos SG, Santos Filho MAB d., Sanz Arnal M, Sar E, Saucède T, Schärer L, Schierwater B, Schilling E, Schmidt-Lebuhn A, Schneider S, Schönberg C, Schrével J, Schuchert P, Schweitzer C, Semple JC, Senna AR, Sennikov A, Serejo C, Shaik S, Shamsi S, Sharma J, Shear WA, Shenkar N, Short M, Sicinski J, Sierwald P, Silva DKF d., Silva ESS, Silva MLCN, Simmons E, Sinniger F, Sinou C, Sivell D, Smit H, Smit N, Smol N, Sørensen MV, Souza-Filho JF, Spelda J, Sterrer W, Steyn HM, Stoev P, Stöhr S, Suárez-Morales E, Susanna A, Suttle C, Swalla BJ, Taiti S, Tanaka M, Tandberg AH, Tang D, Tasker M, Taylor J, Taylor J, Taylor K, Tchesunov A, Temereva E, ten Hove H, ter Poorten JJ, Thirouin K, Thomas JD, Thuesen EV, Thurston M, Thuy B, Timi JT, Todaro A, Todd J, Turon X, Tyler S, Uetz P, Urbatsch L, Uribe-Palomino J, Urtubey E, Utevsky S, Vacelet J, Vader W, Väinölä R, Valdés-Florido A, Valls Domedel G, Van de Vijver B, van Haaren T, van Soest RW, Vanreusel A, Vázquez-García B, Velandia J, Venekey V, Verhoeff T, Villaverde T, Vinarski M, Vonk R, Vos C, Vouilloud AA, Walker-Smith G, Walter TC, Watling L, Wayland M, Wesener T, Wetzel CE, Whipps C, White K, Wieneke U, Williams DM, Williams G, Williams N, Wilson KL, Wilson R, Witkowski J, Wyatt N, Xavier J, Xu K, Zanol J, Zeidler W, Zhao Z, Zullini A. 2024. World Register of Marine Species.

Åkesson B, Gschwentner R, Hendelberg J, Ladurner P, Müller J, Rieger R. 2001. Fission in Convolutriloba longifissura: asexual reproduction in acoelous turbellarians revisited. *Acta Zool* **82**:231–239.

Allard P, Tabin CJ. 2009. Achieving bilateral symmetry during vertebrate limb development. *Semin Cell Dev Biol* **20**:479–484.

Apelt G. 1969. Fortpflanzungsbiologie, Entwicklungszyklen und vergleichende Frühentwicklung acoeler Turbellarien. *Mar Biol* **4**:267–325.

Armed Forces Institute of Pathology. 1960. Manual of histologic staining methods. New York, NY: McGraw-Hill.

Ax P, Schulz E. 1959. Ungeschlechtliche Fortpflanzung durch Paratomie bei acoelen Turbellarien. *Biol Zent Bl* **78**:613–622.

Bailly X, Laguerre L, Correc G, Dupont S, Kurth T, Pfannkuchen A, Entzeroth R, Probert I, Vinogradov S, Lechauve C, Garet-Delmas M-J, Reichert H, Hartenstein V. 2014. The chimerical and multifaceted marine acoel Symsagittifera roscoffensis: from photosymbiosis to brain regeneration. *Front Microbiol* **5**. doi:10.3389/fmicb.2014.00498

Ballarin L, Burighel P, Cima F. 2008. A tale of death and life: natural apoptosis in the colonial ascidian Botryllus schlosseri (Urochordata, Ascidiacea). *Curr Pharm Des* **14**:138–147.

Beltagi S, Mandura A. 1991. Hofstenia arabiensis Nov. Sp. (Hofsteniidae): A New Species of Acoelan Turbellaria from the Red Sea North of Jeddah. *Journal of King Abdulaziz University-science* **3**:65–90.

Bock S. 1923. Eine neue marine Turbellariengattung aus Japan. Almqvist & Wiksell.

Boone M, Houthoofd W, Bert W, Artois T. 2011. First record of Nemertodermatida from Belgian marine waters. *Belg J Zool* **141**:62–64.

Boulan L, Léopold P. 2021. What determines organ size during development and regeneration? *Development* **148**:dev196063.

Bourlat SJ, Hejnol A. 2009. Acoels. *Curr Biol* **19**:R279–280.

Brand JN, Harmon LJ, Schärer L. 2022a. Frequent origins of traumatic insemination involve convergent shifts in sperm and genital morphology. *Evolution Letters* **6**:63–82.

Brand JN, Harmon LJ, Schärer L. 2022b. Mating behavior and reproductive morphology predict

macroevolution of sex allocation in hermaphroditic flatworms. *BMC Biol* **20**:35.
Brand JN, Viktorin G, Wiberg RAW, Beisel C, Schärer L. 2022c. Large-scale phylogenomics of the genus Macrostomum (Platyhelminthes) reveals cryptic diversity and novel sexual traits. *Mol Phylogenet Evol* **166**:107296.
Bush L. 1975. Biology of Neochilda fusca N. gen., n. sp. from the northeastern coast of the United States (Platyhelminthes: Turbellaria). *Biol Bull* **148**:35–48.
Cannon JT, Vellutini BC, Smith J, Ronquist F, Jondelius U, Hejnol A. 2016. Xenacoelomorpha is the sister group to Nephrozoa. *Nature* **530**:89–93.
Charnov EL. 1979. Simultaneous hermaphroditism and sexual selection. *Proc Natl Acad Sci U S A* **76**:2480–2484.
Chiodin M, Børve A, Berezikov E, Ladurner P, Martinez P, Hejnol A. 2013. Mesodermal gene expression in the acoel Isodiametra pulchra indicates a low number of mesodermal cell types and the endomesodermal origin of the gonads. *PLoS One* **8**:e55499.
Corrêa DD. 1960. Two New Marine Turbellaria from Florida. *Bull Mar Sci* **10**:208–216.
Costello HM, Costello DP. 1939. EGG LAYING IN THE ACOELOUS TURBELLARIAN POLYCHOERUS CARMELENSIS. *Biol Bull* **76**:80–89.
Costello HM, Costello DP. 1938. COPULATION IN THE ACŒLOUS TURBELLARIAN POLYCHŒRUS CARMELENSIS. *Biol Bull* **75**:85–98.
Crezee M. 1978. Paratomella rubra Rieger and Ott, an amphiatlantic acoel turbellarian. *Cah Biol Mar* **19**:1–9.
Crezée M. 1975. Monograph of the solenofilomorphidae (Turbellaria: Acoela). *Int Rev Gesamt Hydrobiol* **60**:769–845.
Davies N, Krebs J, West S. 2013. An Introduction to Behavioural Ecology. Wiley-Blackwell.
De Mulder K, Kuales G, Pfister D, Willems M, Egger B, Salvenmoser W, Thaler M, Gorny A-K, Hrouda M, Borgonie G, Ladurner P. 2009. Characterization of the stem cell system of the acoel Isodiametra pulchra. *BMC Dev Biol* **9**:69.
Deng W, Lin H. 2002. Miwi, a murine homolog of piwi, encodes a cytoplasmic protein essential for spermatogenesis. *Dev Cell* **2**:819–830.
Dörjes J. 1968. Die Acoela (Turbellaria) der Deutschen Nordseeküste und ein neues System der Ordnung. *J Zoolog Syst Evol Res* **6**:56–452.
Dörjes J. 1966. Paratomella unichaeta, nov. gen. nov. spec., Vertreter einen neuen Familie der Turbellaria Acoela mit asexueller Fortpflanzung durch Paratomie. *Veröffentlichungen des Instituts für Meeresforschung in Bremerhaven* **II**:187–200.
du Bois-Reymond Marcus E. 1955. On Turbellaria and Polygordius from the Brazilian Coast. *Bol Fac Fil Ci Letr Univ Sao Paulo Zool* **20**:19–53.
Eckelbarger K, Hodgson A. 2021. Invertebrate oogenesis – a review and synthesis: comparative ovarian morphology, accessory cell function and the origins of yolk precursors. *Invertebr Reprod Dev* **65**:71–140.
Falleni A, Gremigni V. 1990. Ultrastructural study of oogenesis in the acoel turbellarian Convoluta. *Tissue Cell* **22**:301–310.
Faubel A. 1983. The Polycladida, Turbellaria. Proposal and establishment of a new system. Part I. The Acotylea. *Mitt Hamb Zool Mus Inst* **80**:17–121.
Faubel A. 1976. Interstitielle Acoela (Turbellaria) aus dem Littoral der nordfriesischen Inseln Sylt und Amrum. *Mitt Hamb Zool Mus Inst* **73**:17–56.
Faubel A. 1974. Die Acoela (Turbellaria) eines Sandstrandes der Nordseeinsel Sylt. *Mikrofauna Meeresbodens* **32**:1–58.
Faubel A, Cameron B. 2001. Platyhelminthes from salt marshes of Coomera River, Southeastern Queensland, Australia. *Mem Queensland Mus* **46**:511–519.
Gardiner E. 1898. The Growth of the Ovum, Formation of the Polar Bodies, and the Fertilization in Polychaerus Caudatus.
Gardiner E. 1895. Early development of Polychoerus Caudatus, Mark. *J Morphol* **11**:155–176.

Gehrke AR, Neverett E, Luo Y-J, Brandt A, Ricci L, Hulett RE, Gompers A, Ruby JG, Rokhsar DS, Reddien PW, Srivastava M. 2019. Acoel genome reveals the regulatory landscape of whole-body regeneration. *Science* **363**:eaau6173.

Giribet G, Edgecombe GD. 2020. The Invertebrate Tree of Life. Princeton University Press.

Gonzalez J, Qi H, Liu N, Lin H. 2015. Piwi is a key regulator of both somatic and germline stem cells in the Drosophila testis. *Cell Rep* **12**:150–161.

Grae D, Kozloff E. 1999. Post-copulatory storage of sperm in the seminal bursa of the acoel flatworm Otocelis luteola. *Invertebr Reprod Dev* **35**:151–154.

Hanson ED. 1960. Asexual Reproduction in Acoelous Turbellaria. *Yale J Biol Med* **33**:107–111.

Harris MP, Daane JM, Lanni J. 2021. Through veiled mirrors: Fish fins giving insight into size regulation. *Wiley Interdiscip Rev Dev Biol* **10**:e381.

Hooge M. 2003. Two new families, three new genera, and five new species of acoels (Acoela Platyhelminthes) from Queensland Australia. *Cah Biol Mar* **44**:275–298.

Hooge M, Smith JPS. 2004. New acoels (Acoela, Acoelomorpha) from North Carolina. *Zootaxa* **442**:1–24.

Hooge M, Wallberg A, Todt C, Maloy A, Jondelius U, Tyler S. 2007. A revision of the systematics of panther worms (Hofstenia spp., Acoela), with notes on color variation and genetic variation within the genus. *Hydrobiologia* **592**:439–454.

Hookabe N, Jimi N, Furushima Y, Fujiwara Y. 2024. Discovery of deep-sea acoels from a chemosynthesis-based ecosystem. *Biol Lett* **20**:20230573.

Hulett RE, Kimura JO, Bolaños DM, Luo Y-J, Rivera-López C, Ricci L, Srivastava M. 2023. Acoel single-cell atlas reveals expression dynamics and heterogeneity of adult pluripotent stem cells. *Nat Commun* **14**:2612.

Hulett RE, Potter D, Srivastava M. 2020. Neural architecture and regeneration in the acoel Hofstenia miamia. *Proceedings of the Royal Society B: Biological Sciences* **287**:20201198.

Hyman LH. 1951. The invertebrates: Platyhelminthes and Rhynchocoela. The acoelomate Bilateria. McGraw-Hill, New York.

Hyman LH. 1937. Reproductive system and copulation in amphiscolops langerhansi (turbellaria acoela). *Biol Bull* **72**:319–326.

Ishikawa K, Yamasu T. 1992. An acoel flat worm species related closely to the species Convolutriloba retrogemma Hendelberg and Akesson occurs in Okinawa Island, Ryukyu Archipelago. *Zoological Science* **9**:1281.

Jehn J, Gebert D, Pipilescu F, Stern S, Kiefer JST, Hewel C, Rosenkranz D. 2018. PIWI genes and piRNAs are ubiquitously expressed in mollusks and show patterns of lineage-specific adaptation. *Commun Biol* **1**:137.

Jondelius U, Wallberg A, Hooge M, Raikova OI. 2011. How the Worm Got its Pharynx: Phylogeny, Classification and Bayesian Assessment of Character Evolution in Acoela. *Syst Biol* **60**:845–871.

Kapli P, Telford MJ. 2020. Topology-dependent asymmetry in systematic errors affects phylogenetic placement of Ctenophora and Xenacoelomorpha. *Sci Adv* **6**:eabc5162.

Kimura JO, Bolaños DM, Ricci L, Srivastava M. 2022. Embryonic origins of adult pluripotent stem cells. *Cell* **185**:4756–4769.e13.

Kimura JO, Ricci L, Srivastava M. 2021. Embryonic development in the acoel Hofstenia miamia. *Development* **148**:dev188656.

Ko JM, Reginato W, Wolff A, Lobo D. 2024. Mechanistic regulation of planarian shape during growth and degrowth. *Development* **151**:dev202353.

Kostenko AG. 1989. The position of Taurida fulvomaculata (Ax, 1959) in the system of Acoela. In: Morphology of turbellarians. *Akad Nauk USSR Trudy Zool* **195**:14–25.

Kozloff EN. 2000a. Differentiation, dedifferentiation, and redifferentiation of reproductive structures of the acoel flatworm*Otocelis luteola*, and notes on longevity of this species. *Invertebr Reprod Dev* **37**:95–106.

Kozloff EN. 2000b. A new genus and five new species of acoel flatworms from the Pacific coast of North America, and resolution of some systematic problems in the families Convolutidae and Otocelididae. *Cah Biol Mar* **41**:281–293.
Kuramochi-Miyagawa S, Kimura T, Ijiri TW, Isobe T, Asada N, Fujita Y, Ikawa M, Iwai N, Okabe M, Deng W, Lin H, Matsuda Y, Nakano T. 2004. Mili, a mammalian member of piwi family gene, is essential for spermatogenesis. *Development* **131**:839–849.
Mamkaev YV. 1965. Etude morphologique d'Actinoposthia beklemischevi n. sp. (Turbellaria Acoela). *Cah Biol Mar* **6**:23–50.
Meyer-Wachsmuth I, Curini Galletti M, Jondelius U. 2014. Hyper-cryptic marine meiofauna: species complexes in Nemertodermatida. *PLoS One* **9**:e107688.
Michiels NK, Newman LJ. 1998. Sex and violence in hermaphrodites. *Nature* **391**:647–647.
Miramón-Puértolas P, Pascual-Carreras E, Steinmetz PRH. 2024. A population of Vasa2 and Piwi1 expressing cells generates germ cells and neurons in a sea anemone. *Nat Commun* **15**:8765.
Peebles F. 1915. A Description of three Acoela from the Gulf of Naples. *Mitteilungen a.d Zool Station zu Neapel* **22**:292–312.
Pellettieri J, Fitzgerald P, Watanabe S, Mancuso J, Green DR, Sánchez Alvarado A. 2010. Cell death and tissue remodeling in planarian regeneration. *Dev Biol* **338**:76–85.
Perea-Atienza E, Botta M, Salvenmoser W, Gschwentner R, Egger B, Kristof A, Martinez P, Achatz JG. 2013. Posterior regeneration in Isodiametra pulchra (Acoela, Acoelomorpha). *Front Zool* **10**:64.
Petrov A, Hooge M, Tyler S. 2004. Ultrastructure of sperms in Acoela (Acoelomorpha) and its concordance with molecular systematics. *Invertebr Biol* **123**:183–197.
Philippe H, Brinkmann H, Copley RR, Moroz LL, Nakano H, Poustka AJ, Wallberg A, Peterson KJ, Telford MJ. 2011. Acoelomorph flatworms are deuterostomes related to Xenoturbella. *Nature* **470**:255–258.
Raikova O, Falleni A, Gremigni V. 1995. Oogenesis in Actinoposthia beklemischevi (Platyhelminthes, Acoela): an ultrastructural and cytochemical study. *Tissue Cell* **27**:621–633.
Ramm SA, Schlatter A, Poirier M, Schärer L. 2015. Hypodermic self-insemination as a reproductive assurance strategy. *Proceedings of the Royal Society B: Biological Sciences* **282**:20150660.
Reddien PW. 2018. The cellular and molecular basis for planarian regeneration. *Cell* **175**:327–345.
Ricci L, Srivastava M. 2021. Transgenesis in the acoel worm Hofstenia miamia. *Dev Cell* **56**:3160–3170.e4.
Rieger RM, Tyler S, Smith JPS, Rieger GE. 1991. Platyhelminthes and NemertineaMicroscopic Anatomy of Invertebrates. New York: Wiley-Liss. pp. 7–140.
Riser NW. 1987. Nemertinoides elongatus gen. n., sp. n. (Turbellaria: Nemertodermatida) from coarse sand beaches of the Western North Atlantic. *Proc Helminthol Soc Wash* **54**:60–67.
Rychel AL, Swalla BJ. 2008. Anterior regeneration in the hemichordate Ptychodera flava. *Dev Dyn* **237**:3222–3232.
Sagata N. 1996. Meiotic metaphase arrest in animal oocytes: its mechanisms and biological significance. *Trends Cell Biol* **6**:22–28.
Schärer L, Janicke T, Ramm SA. 2014. Sexual conflict in hermaphrodites. *Cold Spring Harb Perspect Biol* **7**:a017673.
Schärer L, Littlewood DTJ, Waeschenbach A, Yoshida W, Vizoso DB. 2011. Mating behavior and the evolution of sperm design. *Proceedings of the National Academy of Sciences* **108**:1490–1495.
Schmidt-Rhaesa A. 2007. The Evolution of Organ Systems. OUP Oxford.
Shannon T, Achatz J. 2007. Convolutriloba macropyga sp. nov., an uncommonly fecund acoel

(Acoelomorpha) discovered in tropical aquaria. *Zootaxa* **1525**:1–17.
Srivastava M. 2022. Studying development, regeneration, stem cells, and more in the acoel Hofstenia miamia. *Curr Top Dev Biol* **147**:153–172.
Srivastava M, Mazza-Curll KL, van Wolfswinkel JC, Reddien PW. 2014. Whole-Body Acoel Regeneration Is Controlled by Wnt and Bmp-Admp Signaling. *Curr Biol* **24**:1107–1113.
Steinböck O. 1966. Grundsätzliches zur Evolution der Turbellarien. *Zeitschrift für Zoologische Systematik und Evolutionsforschung* **4**:58–195.
Sterrer WE. 1998. New and known Nemertodermatida (Platyhelminthes- Acoelomorpha) - a revision. *Belgian Journal of Zoology* **128**:55–92.
Tong SJW, Ong RSL. 2020. Mating behavior, spawning, parental care, and embryonic development of some marine pseudocerotid flatworms (Platyhelminthes: Rhabditophora: Polycladida) in Singapore. *Invertebr Biol* **139**:e12293.
Trible W, Kronauer DJC. 2017. Caste development and evolution in ants: it's all about size. *J Exp Biol* **220**:53–62.
Tyler, S., Schilling, S., Hooge, M., & Bush, L. F. 2012. Turbellarian taxonomic database. Version 1.7. http://turbellaria.umaine.edu
Uppaluri S, Brangwynne CP. 2015. A size threshold governs Caenorhabditis elegans developmental progression. *Proc R Soc B* **282**:20151283.
Vallejo DM, Juarez-Carreño S, Bolivar J, Morante J, Dominguez M. 2015. A brain circuit that synchronizes growth and maturation revealed through Dilp8 binding to Lgr3. *Science* **350**:aac6767.
Wallberg A. 2012. The Stylet - Diversity and Systematics of Acoela and Nemertodermatida. http://acoela.myspecies.info
Watzin MC. 1984. Egg Laying in the Acoel Turbellarian Neochildia fusca. *Trans Am Microsc Soc* **103**:322–325.
Wolpert L. 2010. Arms and the man: the problem of symmetric growth. *PLoS Biol* **8**:e1000477.
Zabotin YI, Evtugyn VG. 2021. Ultrastructure of spermatozoa and female copulatory organs in preferably asexually-reproducing acoel Convolutriloba retrogemma (Acoelomorpha). *Zoomorphology* **140**:19–26.
Zauchner T, Salvenmoser W, Egger B. 2015. A cultivable acoel species from the Mediterranean, Aphanostoma pisae sp. nov. (Acoela, Acoelomorpha). *Zootaxa* **3941**:401–413.